United States
Environmental Protection
Agency

Office of Research and
Development
Washington DC 20460

EPA/600/R-01/007b
March 2001

Multispecies Reactive Tracer Test in a Sand and Gravel Aquifer, Cape Cod, Massachusetts

Part 2

Transport of Chromium (VI) and Lead-, Copper-, and Zinc-EDTA Tracers

EPA/600/R-01/007b
March 2001

Multispecies Reactive Tracer Test in a Sand and Gravel Aquifer, Cape Cod, Massachusetts

Part 2

Transport of Chromium(VI) and Lead-, Copper, and Zinc-EDTA Tracers

J. A. Davis[1], J. A. Coston[1], D. B. Kent[1], K. M. Hess[2], J. L. Joye[1], P. Brienen[1] and K. W. Campo[2]

[1] U.S. Geological Survey
Menlo Park, CA 94025

[2] U.S. Geological Survey
Northborough, MA 01532

Interagency Agreement DW14935626

Project Officer
Robert W. Puls
Subsurface Protection and Remediation Division
National Risk Management Research Laboratory
Ada, OK 74820

National Risk Management Research Laboratory
Office of Research and Development
U.S. Environmental Protection Agency
Cincinnati, OH 45268

Notice

The U. S. Environmental Protection Agency through its Office of Research and Development partially funded and collaborated in the research described here under Interagency Agreement DW14935626. It has been subjected to the Agency's peer and administrative review and has been approved for publication as an EPA document. Mention of trade names or commercial products does not constitute endorsement or recommendation for use.

All research projects making conclusions or recommendations based on environmentally related measurements and funded by the Environmental Protection Agency are required to participate in the Agency Quality Assurance Program. This project was conducted under an approved Quality Assurance Project Plan. The procedures specified in this plan were used without exception. Information on the plan and documentation of the quality assurance activities and results are available from the Principal Investigator.

Foreword

The U.S. Environmental Protection Agency is charged by Congress with protecting the Nation's land, air, and water resources. Under a mandate of national environmental laws, the Agency strives to formulate and implement actions leading to a compatible balance between human activities and the ability of natural systems to support and nurture life. To meet this mandate, EPA's research program is providing data and technical support for solving environmental problems today and building a science knowledge base necessary to manage our ecological resources wisely, understand how pollutants affect our health, and prevent or reduce environmental risks in the future.

The National Risk Management Research Laboratory (NRMRL) is the Agency's center for investigation of technological and management approaches for preventing and reducing risks from pollution that threatens human health and the environment. The focus of the Laboratory's research program is on methods and their cost-effectiveness for prevention and control of pollution to air, land, water, and subsurface resources; protection of water quality in public water systems; remediation of contaminated sites, sediments and ground water; prevention and control of indoor air pollution; and restoration of ecosystems. NRMRL collaborates with both public and private sector partners to foster technologies that reduce the cost of compliance and to anticipate emerging problems. NRMRL's research provides solutions to environmental problems by: developing and promoting technologies that protect and improve the environment; advancing scientific and engineering information to support regulatory and policy decisions; and providing the technical support and information transfer to ensure implementation of environmental regulations and strategies at the national, state, and community levels.

The use of multispecies reactive transport modeling in site assessments and remedial performance monitoring at hazardous waste sites is to be encouraged. These can be valuable tools for simulating processes which govern contaminant fate and transport in the subsurface. A competent reactive transport model of a site must be able to simulate the processes that occur between water and the vapor and solid phases in contact with the water. The accuracy of such simulations will be dependent on the database contained within such models as well as the quality of the site-specific data collection efforts.

The lessons learned from the large-scale tracer tests and subsequent modeling investigations from this study have implications that go far beyond the particular contaminant species studied here. For homogeneous and classical heterogeneous reactions (e.g., dissolution equilibria), there are generally available equilibrium constants that may be used with confidence in such models; however, solubilities for poorly crystalline or impure solid phases are generally not available and will have to be determined using site-specific materials. Adsorption and other heterogeneous surface reactions will generally require experimental determination of parameters that are site-specific. In addition, chemical reactions can be rate-limited and controlled by physical factors such as diffusion or mixing of waters across sediment layers. These studies were important in identifying the limitations of reactive transport modeling, their utility, and where additional data collection and testing is warranted.

Stephen G. Schmelling, Acting Director
Subsurface Protection and Remediation Division
National Risk Management Research Laboratory

Executive Summary

A comprehensive field investigation of multispecies reactive transport under variable chemical conditions was conducted in a shallow, unconfined, sand and gravel aquifer, on Cape Cod, Massachusetts. Ten thousand liters of groundwater with added tracers were injected into the aquifer, and the distributions of tracers were monitored for more than one year as the tracers were transported over 200 meters (m) through an array of multilevel samplers (MLS). Tracers included a nonreactive tracer (bromide ion) and the reactive solutes Cr(VI) and EDTA (ethylenediaminetetraacetic acid) complexes of the divalent metal ions, Ni, Cu, Zn, and Pb. The EDTA concentration in the injected water was in slight excess of the sum of the four metals, ensuring that the speciation of the injected metals was dominated by their EDTA complexes. Transport of the tracers was quantified using spatial moments computed from a series of comprehensive synoptic samplings of the tracer cloud and temporal moments of concentration data collected frequently at two MLS (breakthrough curves).

The vertical interval over which the tracers were injected spanned three zones with contrasting chemical conditions. The *pristine zone*, with high concentrations of dissolved oxygen (DO), pH values in the range 5.4-5.7, and low concentrations of dissolved salts, overlaid the *sewage-contaminated zone*, with low concentrations of DO (< 3 μM) and dissolved manganese, pH values in the range 6.0-6.5, and increased concentrations of dissolved salts and sewage-derived contaminants, such as phosphate and Zn. Between the pristine and sewage-contaminated zones was the *Zn-contaminated region*, with elevated concentrations of dissolved and adsorbed Zn derived from the sewage effluent. The Zn-contaminated region was approximately 3 m thick near the injection location but decreased in thickness with distance downgradient. Concentrations of dissolved and adsorbed Zn decreased with distance downgradient, until at 150 m away from the injection, no Zn contamination in the aquifer could be detected.

Chemical interactions between the reactive tracers and the aquifer sediments varied among the different solutes and the different geochemical zones. More spreading and greater retardation of Cr(VI) and the metal-EDTA complexes was observed in the pristine zone as a result of increased adsorption of these anionic solutes in that zone. The most important factors favoring adsorption in the pristine zone relative to the other zones were the lower pH value and lower concentrations of other anions that could compete for adsorption sites on the surfaces of the sediments.

Transport of the metal-EDTA complexes was affected by the extent and rates of various metal exchange reactions, in which the metal ion of one of the injected metal-EDTA complexes was displaced by another cation, such as Fe, Al, or Zn in the Zn-contaminated region of the aquifer. The free metal ions produced as a product of such metal exchange reactions, such as Pb^{2+}, were extensively adsorbed under the chemical conditions present in the aquifer. Fe and Al was made available as a reactant for the metal exchange reactions by dissolution of poorly crystalline oxyhydroxide phases present as coatings on the Cape Cod sediments.

The metal exchange reactions of Pb-EDTA complexes appeared to be the most thermodynamically favored in the aquifer, although the extent of Zn-EDTA metal exchange was also significant outside of the region of Zn contamination. Because of the strong adsorption of Pb^{2+} released in the metal exchange reactions of Pb-EDTA complexes, the mass of dissolved Pb within the tracer cloud decreased rapidly and was not detectable 110 days after the injection. Pb-EDTA complexes primarily exchanged EDTA with Zn and Fe(III) in the first 13 days after the injection, with the Fe derived from dissolution of sediment coatings and Zn derived from desorption within the Zn-contaminated region. Al-EDTA complexes that had formed with excess EDTA shortly after the injection also exchanged with Fe. Dissolved Al-EDTA complexes were not detectable 83 days after the injection. The dissolved mass of Fe-EDTA complexes increased steadily throughout the tracer test; the rate of Fe dissolution appeared to be rate-limited at the beginning of the tracer test.

The metal exchange reactions of Cu-EDTA complexes continued slowly throughout the tracer test, and approximately 30% of the injected Cu-EDTA was still present in the tracer cloud 300 days after the injection. The net mass of dissolved Zn-EDTA in the tracer cloud increased during the first 175 days of the tracer test, due to desorption of contaminant Zn from the sediments and the formation of dissolved Zn-EDTA complexes. However, outside of the Zn-contaminated region, dissolved Zn-EDTA was lost from the tracer cloud as a result of metal exchange reactions with Fe(III). During the period 175 to 300 days after the injection, the mass of dissolved Zn-EDTA decreased rapidly as the balance shifted to a net loss of Zn-EDTA in the metal exchange reactions. The loss of Zn-EDTA increased as the tracer cloud sank below the Zn-contaminated region and was transported longitudinally beyond the region with greatest Zn-contamination.

The order of displacement of the metal ions (Pb>>Zn>Cu>>Ni) observed within the pristine and suboxic zones is consistent with thermodynamic predictions that consider both the strength of the aqueous EDTA complexes and the strength of adsorption of the free metal ions. At chemical equilibrium and in groundwater saturated with ferrihydrite, the thermodynamic calculations show that the extent of the metal exchange reactions depends on both pH and the concentration of the metal-EDTA complex. This couples the extent of the metal exchange reactions with dispersion and other processes that lower the concentration of the metal-EDTA complexes in the groundwater.

Loss of dissolved Cr(VI) from the tracer cloud was observed as a result of the reduction of Cr(VI) to Cr(III), and irreversible sorption of Cr(III). This occurred primarily in the sewage-contaminated zone, in agreement with the results of small-scale tracer tests previously conducted at the site. Adsorption of the anionic Cr(VI) species in the pristine zone resulted in significant retardation and spreading. Retardation of Cr(VI) was dependent on chemical conditions that correlated well with the chemical gradients as a function of altitude. Quantitative description of the loss of Cr(VI) from the tracer cloud will likely require accounting for the sinking of the tracer cloud across the oxic-suboxic boundary that occurred during the course of the experiment.

The fate and transport of Zn in the sewage effluent were well described by a multispecies reactive transport model that included surface complexation reactions to describe the pH dependence of Zn adsorption. Reasonable quantitative predictions of the distribution of Zn contamination at the field site were made from simulations in which the surface complexation model parameters were calibrated from the results of laboratory batch experiments. These simulations, as well as other preliminary modeling investigations presented here, will serve as a starting point for reactive transport modeling of the experimental results of the tracer test. The results of the field experiment provide a well-characterized, chemically complex data set that can stimulate the development and testing of hydrogeochemical transport models of flow coupled with chemical reactions.

Contents

Tables

Figures

Abbreviations

d	Day
DO	dissolved oxygen
EDTA	ethylenediaminetetraacetic acid
g	Grams
ICP-AES	inductively-coupled plasma atomic emission spectroscopy
kg	Kilograms
km	Kilometers
L	Liters
m	Meter
µg	Micrograms
µM	Micromoles per liter
mg	Milligrams
mM	Millimoles per liter
mm	Millimeters
M	Moles
MLS	multilevel sampler
nm	Nanometers
QC	quality control

SI Conversion Factors

Multiply	English (US) Units	by	Factor	to get	Metric (SI) Units
Area:	1 ft^2		0.0929		m^2
	1 in^2		6.452		cm^2
Flow rate:	1 gal/min		6.31×10^{-5}		m^3/s
	1 gal/min		0.0631		L/s
	1 MGD		43.81		L/s
Length:	1 ft		0.3048		m
	1 in		2.54		cm
Mass:	1 lb		453.59		g
	1 lb		0.45359		kg
Volume:	1 ft^3		28.316		L
	1 ft^3		0.028317		m^3
	1 gal		3.785		L
	1 gal		0.003785		m^3
Temperature:	^oF - 32		0.55556		^oC
Concentration:	1 gr/ft^3		2.2884		g/m^3
	1 gr/gal		0.0171		g/L
	1 lb/ft^3		16.03		g/L
Pressure:	1 lb/in^2		0.07031		kg/cm^2
	1 lb/in^2		6894.8		Newton/m^2
Heating value:	Btu/lb		2326		Joules/kg
	Btu/scf		37260		Joules/scm

Acknowledgments

We are grateful to Drs. Barbara Bekins, John Friedly, and Juerg Zobrist for critical technical reviews of the report. Numerous people contributed to the field and laboratory work reported here. Technical and field assistance were provided by Steve Coppola, Bill Carothers, Greg Granato, Matthias Kohler, Mary Kruger, John Masterson, Tim McCobb, Bill Mitch, Brigid Rea, and Jennifer Savoie, sometimes under unfavorable conditions. Charlie Ogle (Ogle Tooling) and Mike Fitzgerald (Design Craft Woodworks) provided critical assistance in the design and construction of the apparatus used for processing “Chelex” samples. Sean Wallace conducted laboratory experiments on chemical interactions between EDTA and aquifer sediments described in the text. Chris Fuller and Linda Anderson provided technical advice on experimental design, sampling, and analysis at various stages during the project. The numerous contributions of Denis LeBlanc, USGS Cape Cod Groundwater Research Site Coordinator, and Dr. Robert Puls, Project Officer, U.S. Environmental Protection Agency, are gratefully acknowledged. Funding for the project was provided by the U.S. Environmental Protection Agency, through interagency agreement number DW14935626 and the U.S. Geological Survey Toxic Substances Hydrology Program.

Introduction

Chemical speciation can have a major influence on the transport of inorganic solutes (Davis et al., 1993b; Yeh and Tripathi, 1991; Liu and Narasimhan, 1989). As an example, free (uncomplexed) metal ions such as zinc (Zn) are extensively retarded in groundwater (von Gunten et al., 1991; Kent et al., 2000). In contrast, the formation of weakly adsorbing, anionic complexes greatly increases the mobility of metal ions, as in the cases of Zn (Kent et al., 1992) or cobalt (Co, Zachara et al., 1995b) complexed with ethylenediaminetetraacetic acid (EDTA). Other examples of mobile and weakly adsorbing organic complexes are found in groundwater studies of copper (Cu) and a variety of radionuclides (McCarthy et al., 1998; McBride et al., 1997; Jacobs et al., 1988; von Gunten et al., 1991; Killey et al., 1984). Changes in pH along groundwater flow paths can also cause shifts in metal ion speciation that affect mobility.

In addition to complexation and acid-base reactions, redox (electron transfer) reactions may cause changes in speciation that have a marked effect on transport. Aqueous chromium (VI) species (Cr, in the plus six oxidation state) are generally soluble and relatively weakly adsorbing, hence they can be mobile in groundwater (Kent et al., 1995). Cr(III), if uncomplexed, should be highly retarded in groundwater because its aqueous species are extensively adsorbed or insoluble (Kent et al., 1994; Anderson et al., 1994).

This report discusses the transport of a group of reactive tracers over the course of a large-scale, natural gradient tracer test conducted at the USGS Cape Cod Toxic Substances Hydrology Research site, near Falmouth, Massachusetts (Davis et al., 2000a,b). The overall objectives of the experiment were to demonstrate the importance of variable aquifer chemistry on chemical reactions, including aqueous speciation changes, during transport of toxic elements in groundwater (chromate, and four metals complexed with the organic ligand EDTA: Pb, Cu, Zn, Ni). In addition, the field experiment was designed to collect enough data to investigate the problem of modeling flow coupled with chemical reactions with a view towards simplification of the geochemical reaction network.

The variable chemical conditions at the field site and the transport of conservative Br and weakly reactive Ni-EDTA complexes are described in a companion report (Davis et al., 2000a). The main conclusions of the companion report were that: 1) Br was transported conservatively; 2) EDTA and Ni-EDTA were reversibly adsorbed to the aquifer sediments during transport, with only slight retardation relative to Br; 3) the masses of total dissolved EDTA and Ni were nearly constant during the tracer test after the initial adsorptive equilibrium was reached; and 4) the injected metals, except for Zn and Cr, were transported entirely as metal-EDTA complexes (Davis et al., 2000a,b). Observed tracer retardation was most extensive under the low pH conditions of the pristine zone, a conclusion consistent with earlier smaller scale tracer studies of metal-EDTA complexes (Kent et al., 1992; Kent et al., in preparation).

Methods and Materials

A field site was chosen where the mobility of reactive tracers under variable chemical conditions could be compared, and the fate of the tracers in response to different chemical processes could be contrasted. The hydrogeology, geochemistry and injection design were discussed extensively in the companion report (Davis et al., 2000a). Only a brief description of the pertinent details is included here.

Site Description

The study site is located in a shallow, unconfined sand and gravel aquifer, that is part of a large sand and gravel outwash plain deposited during the retreat of a continental glacier about 15,000 years ago (Oldale and Barlow, 1986) on Cape Cod, Massachusetts (see Figure 1, Davis et al., 2000a). The sediments were primarily Fe and Al oxyhydroxide coated quartz (90-95%), with minor amounts of K-feldspar and ferromagnetic minerals. The fine fraction (<64 microns) represented about 1% by weight of the sediments and the mass of organic carbon was ≤0.01%. Carbonate minerals were not present in the sediments. The average aquifer porosity was 0.39.

The study site has an array of over 800 multilevel samplers oriented along the average flow direction (Figure 1), which will be discussed further below. The water table was 4 - 7 m below land surface and sloped to the south at 1.6 m per 1000 m. Shallow groundwater at the site was contaminated by secondary sewage effluent that was discharged from 1936 through 1995 onto infiltration beds located about 240 m upgradient of the injection wells. The contaminated water formed a plume that extended up to 5 km south of the infiltration beds. Vertical concentration gradients in dissolved oxygen (DO), pH, dissolved Zn, and other water quality parameters were observed near the water table; these gradients were caused by the mixing of the sewage effluent with pristine, recharge water (Kent et al., 1994; Kent et al., submitted) (Figure 2). Chemical conditions in the upper portion of the sewage-contaminated region were mildly reducing: Fe(II) concentrations were below detection, DO was extremely low, and there were significant concentrations of dissolved manganese (Mn) and nitrate. These conditions are referred to as suboxic. Figure 2 shows typical chemical profiles in the aquifer near the water table and at the top of the sewage-contamination plume. Longitudinal contours of the background geochemical conditions in the aquifer, constructed from concentration data collected prior to the tracer test, were published in Davis et al. (2000a,b).

For discussion purposes, we have defined three zones of chemical conditions in the groundwater: 1) a *pristine zone* of uncontaminated, recharge water, 2) a *sewage-contaminated zone* that is suboxic, and 3) an approximately 2.5 m thick *Zn-contaminated region* between the other two zones that includes the region where chemical gradients occurred in DO and other solute concentrations (Figure 3). The pristine zone is the region near the water table where the groundwater was close to or at saturation with DO (corresponding to an elevation of 12.5 m or greater). The sewage-contaminated zone is defined as the region where the dissolved oxygen was approximately zero ($\leq$3 μM) and the background dissolved Zn was below detection (<0.15 μM), roughly corresponding to an elevation of 10 m or less. The Zn-contaminated region incorporates the gradients in DO and dissolved salt concentrations, since it was coincident with the zone of mixing between the sewage-contaminated and pristine groundwaters.

Zn Partitioning in the Zn-contaminated Region of the Aquifer

A typical vertical profile had a peak in dissolved Zn concentration near the upper boundary of the sewage plume, in the region where the pristine and sewage-contaminated waters mix (Figure 2). The size, shape, and Zn concentrations in the Zn-contaminated region varied with distance downgradient (Kent et al., 2000). Figure 4 shows Zn concentrations and pH values along a longitudinal cross section originating at the injection location. In addition to the longitudinal trends, there were lateral variations in the shape of the Zn-contaminated region. These variations are illustrated in Figure 5. From the center of the injection to about 75 m downgradient, both the thickness of the Zn-contaminated region and the peak concentrations of dissolved Zn increased from west to east across the part of the aquifer traversed by the tracer cloud. The locations of the upper and lower boundaries varied from west to east throughout the Zn-contaminated region.

Dissolved Zn concentrations in the groundwater were buffered by a reservoir of Zn adsorbed on the aquifer sediments. Rea et al. (1991) used hydroxylamine-hydrochloride (HH) extractions of aquifer sediments to show the peak in extracted Zn coincides with the location of the dissolved Zn peak in the groundwater. The amount of extracted Zn on the sediments was approximately two orders of magnitude greater than that of dissolved Zn (per unit bulk volume of aquifer). Results of small-scale tracer tests with free EDTA injected at various depths in the aquifer corroborate the HH extraction data (Kent et al., 1992; Kent et al., in preparation). When free EDTA was injected into the Zn-contaminated region, the mass of Zn relative to that of conservative tracers increased with distance downgradient (Davis et al, 1993b). No increase in Zn mass was observed when free EDTA was injected deeper in the sewage plume, below the region with dissolved Zn (Kent et al., 1992).

The distribution of Zn in the aquifer was controlled by pH-dependent adsorption onto aquifer sediments. Under the chemical conditions present in the aquifer, Zn-bearing mineral phases, such as hydroxides, carbonates, and phosphates, were undersaturated by several orders of magnitude (Rea et al., 1996). Laboratory studies have shown that the partitioning of Zn between the sediments and artificial groundwater is consistent with adsorption of Zn onto the Fe and Al oxyhydroxide coatings on the sediment grains (Coston et al., 1995). Experimental data on partitioning of Zn onto aquifer sediments were well described by a simple surface complexation model (Davis et al., 1998). Figure 6 shows dissolved Zn concentration as a function of pH for various concentrations of total Zn, computed using the surface complexation model. For a given value of total Zn (adsorbed plus dissolved Zn), the computed dissolved Zn decreases substantially with increasing pH. Also shown in Figure 6 are data from two multilevel samplers less than 1 m apart, which were sampled in 1991 and 1993 at the elevations where the highest dissolved Zn concentrations were observed (11.3 to 12.0 m, Figure 2). Dissolved Zn concentrations were higher and pH values lower in June of 1991 than in April of 1993. Despite the differences in the observed dissolved Zn concentrations, the surface complexation model simulations suggest that these field data were consistent with the Zn partitioning expected for a total Zn concentration of approximately 80 μM per liter of groundwater.

Tracer Test Experimental Design

The test site had an array of over 809 multilevel samplers (MLS) oriented along the average flow direction (LeBlanc et al., 1991). Each MLS consisted of 15 sampling ports spaced between 25 and 76 cm apart, creating a vertically dense set of sampling ports across the extant geochemical gradients. Groundwater, spiked with seven tracers (see below), was injected simultaneously at 3 depths, 1 meter apart, into six MLS installed for the experiment (shown in the inset of Figure 1). The injection was designed so that a portion of the tracer cloud traveled in each of the aquifer zones depicted in Figure 3.

In April 1993, 9,884 liters of pristine groundwater were pumped into an above ground plastic-lined pool, and the following tracers were added: bromide (Br, 3.43 mM), chromate (Cr(VI), 0.506 mM), and four metals (Pb, 0.248 mM; Cu, 0.266 mM; Ni, 0.256 mM; Zn, 0.266 mM) complexed with ethylenediaminetetraacetic acid (EDTA, 1.112 mM). A small excess of EDTA (7%) was present in the injectate. The predominant species of the reactive tracers in the injectate water were $HCrO_4^-$, $PbEDTA^{2-}$, $CuEDTA^{2-}$, $NiEDTA^{2-}$, and $ZnEDTA^{2-}$. Adsorption of these anions is dependent on pH and the concentration of competing anions, as observed in previous tracer tests (Kent et al., 1992; 1994; 1995; in preparation) and in laboratory studies (Bowers and Huang, 1986; Huang et al., 1988; Borggaard, 1991; Nowack and Sigg, 1996). It was expected that: 1) metal exchange reactions involving Fe(III) and the metal-EDTA complexes would occur in the aquifer, releasing uncomplexed tracer metal ions, e.g. Pb^{2+}, to the system; and, 2) Cr(VI) would be reduced to the immobile species Cr(III) under suboxic conditions.

Synoptic samplings were conducted for nine months after the injection. A longitudinal transect with pH, and metal speciation data was also collected during the synoptic sampling rounds. Temporal sampling was conducted at two breakthrough MLS, 37 and 52 m downgradient from the injection site (Figure 1), where samples were collected frequently and analyzed for Br, EDTA, total metals and Chelex-filtered metals (Davis et al., 2000a). These MLS are referred to as BT1 and BT2, respectively. As shown in Figure 4, the sampling ports of these MLS spanned from the pristine zone to the sewage-contaminated zone and across a pH gradient from 5.4 to 6.2. Both MLS sampled the Zn-contaminated region at the middle ports and extended well above and below the region at the top and bottom ports.

Laboratory Batch Studies of Fe and Al Dissolution by EDTA

In order to determine the short-term rate of Fe and Al dissolution and Zn desorption by EDTA, a series of experiments using aquifer sediments collected from the different aquifer zones were completed. The experiments were designed to study reactions that may have occurred during the first 12 days of the tracer test, prior to the first synoptic sampling.

Core material was collected from the aquifer in 1994 along a transect 2 m east of the MLS array, using a wireline-piston core barrel and plastic core liners approximately 1.5 m in length (Zapico et al., 1987). Cores were frozen immediately after collection, and stored frozen until processed. Each core was sectioned at 10 cm intervals, dried under a laminar flow hood at room temperature, and then sieved to remove grains >1 mm in diameter. A sample of the <1 mm material from each core section was leached with HH at 50°C for 30 minutes (after Chao and Zhou, 1983) to determine the amount of amorphous iron and aluminum oxyhydroxides. The amount of Zn extracted in each subsample was used to determine which intervals represented the Zn-contaminated region in the cores. Three composite samples, representative of the pristine, Zn-contaminated, and sewage-contaminated zones, were prepared by mixing the appropriate sieved and dried subsections. BET surface areas were measured by nitrogen gas adsorption (after Coston et al., 1995).

The dissolution experiments used two different artificial groundwater solutions: pristine artificial groundwater (PAGW, Anderson et al., 1994) and sewage-contaminated artificial groundwater (SAGW, Coston et al., 1995). The composition of the artificial ground waters approximated the average concentrations of the major ions, such as calcium, magnesium, potassium, chloride and sulfate. pH was controlled by the addition of 2-N-morpholinoethane sulfonic acid (MES) buffer to the artificial groundwater solutions. PAGW was adjusted to pH 5.4 and SAGW was adjusted to pH 6.5. Primary EDTA (Na_4EDTA) solutions were made up at least 2 days in advance and stored in the dark.

Since the sediments were dried, the experiments included a pre-equilibration procedure in the pH-adjusted artificial groundwater (Coston, et al. 1995). All batch experiments had a solid to solution ratio of 400 grams of sediment per liter of artificial groundwater. After pre-equilibration, EDTA was added from the primary standards, the tubes were covered in foil and mounted on end-over-end rotators for the desired reaction time (0.5 to 336 hours). The total concentration of EDTA added was 0.10 mM in each tube. At the end of a reaction period, the pH was measured, and the samples centrifuged at 24,000*g*. Three aliquots of supernatant were collected from each tube for chemical analyses: 1) EDTA concentration, 2) cation concentrations, and 3) metal speciation samples.

Chemical Analyses

Samples were analyzed by a variety of different methods to determine the total and speciated concentrations of the tracers. Bromide was determined colorimetrically (by flow injection analysis) on unfiltered samples (Franson, 1985). An aliquot of the same unfiltered sample was used to determine EDTA using the spectrophotometric method of Bhattacharyya

and Kunda (1971). Metal analyses were made on filtered (0.45 micrometer) and acid preserved samples by ICP-AES (Coston et al., 1998). Free metal ion tracer concentrations were determined in filtered water samples exchanged with Chelex-100 resin, then acidified and measured by ICP-AES. The concentration of Cr(VI) was measured colorimetrically in a small subset of anion samples by the addition of diphenylcarbazide and HCl (Franson, 1985). The method has been used successfully in previous groundwater studies at the site (Kent et al., 1994, 1995; Anderson et al., 1994). The concentration of Cr(VI) measured was always found to be equivalent to the total Cr concentration as measured by ICP-AES. Additional details about the chemical analyses were included in the companion report to this publication (Davis et al., 2000a).

Iron-containing colloidal material has been reported to exist within the sewage-contaminated zone at the site. Gschwend and Reynolds (1987) detected ferrous phosphate particles approximately 0.1 micrometers in diameter in the anoxic zone (containing dissolved Fe(II), Kent et al., 1994) of the sewage plume. The tracer cloud did not enter the anoxic zone, and, therefore this material could not have caused an observance of dissolved Fe in the samples. Sampling and filtration experiments showed that small concentrations of Fe (less than 0.5 μM) derived from Fe-containing particles could be detected in unfiltered samples at some locations in the suboxic zone (Kent, 1998). These were removed by 0.45 micrometer but not 8.0 micrometer filters. Laboratory column experiments conducted with sediments from the Cape Cod aquifer have shown that a 1000-fold decrease in ionic strength did not significantly mobilize colloidal material. However, an increase in pH from 4.8 to 6.3 did mobilize a small concentration of silica-rich colloids in the size range 0.4 to 0.8 micrometers (Roy and Dzombak, 1996, 1997). As was observed in sampling and filtration experiments, material in this size range would have been filtered out prior to acidification of groundwater samples. Additionally, increases in pH of this magnitude associated with passage of the tracer cloud were only observed within a few meters of the injection in the pristine zone (Davis et al., 2000a). Fluctuations in pH during breakthrough of tracers in the suboxic zone and in all zones farther downgradient of the injection were negligible (Davis et al., 2000a). Thus, it is very unlikely that mobilization of colloids contributed significantly to the observations of dissolved Fe or Al later in the tracer test.

Spatial and Temporal Moments

The transport parameters of the solutes were quantified from both spatial and temporal data sets. Spatial-moments estimated tracer mass, location, velocity, and other transport parameters for each synoptic sampling. Results for Br, Ni and EDTA and details of the integration approach are presented in the companion report (Davis et al., 2000a).

The analysis included here does not correct the computed values of dissolved Zn mass for any Zn mass included from the background concentrations of dissolved Zn^{2+}. Unlike the other tracers, the boundaries of the spatial integration for Zn could not be defined by concentrations that fell below the detection limit. Instead, for each spatial sampling, the Zn moments were calculated with the same boundaries used for the calculation of Ni mass. It is possible that the Zn-EDTA cloud was smaller than Ni-EDTA for some of the spatial samplings. Because the spatial integration was extended to the side boundaries where Ni concentrations were zero, some Zn dissolved mass would have been included within that area due to nonzero background Zn^{2+} concentrations. As the tracer cloud spread longitudinally with time, the number of MLS required to establish the side tracer cloud boundaries increased, and thus the contribution of background Zn^{2+} concentrations to the calculated dissolved Zn mass probably increased.

Tracer was detected in all but the uppermost ports of each of the breakthrough MLS. At both MLS, some of the injected tracers and Fe were detectable over a broader altitude range than Br. For example, at BT1, Cr, Cu, Fe and Zn were detected at 13.21 m, 0.3 m above the highest elevation where Br was measured. At BT2, where sampling ports extended deeper into the aquifer, Zn- and Fe-EDTA complexes were measurable up to 1 meter below the lowest elevation with measurable Br. Due to the density contrast between the injectate solution and the ambient ground water, center of mass of Br tracer sank about 1.9 m during transport (Davis et al., 2000a,b). The distribution of metals at the breakthrough MLS was also consistent with some vertical retardation of the reactive tracers during sinking. The normalized breakthrough curves (measured concentration/injected concentration: C/C_o) were analyzed using the trapezoidal integration method (Roberts et al., 1986; Harvey and Garabedian, 1991; Kent et al., 1994, 1995). These results are presented in Tables 1-4.

Results and Discussion

Spatial and Temporal Distribution of Reactive Tracers During Transport

Longitudinal contours of the injected tracers at 13 and 83 days after injection (Figures 7 and 8, respectively) illustrate the results of reactive transport during the experiment. Differences between the distribution of reactive and nonreactive tracers among the aquifer zones were already apparent after 13 days (Figure 7). The most striking example was for the Pb tracer. At 13 days, the Pb cloud presented the most compact outer contour of all the injected tracers. Seventy days

later, only a small amount of Pb persisted in the sewage-contaminated zone (Figure 8). In contrast, both Ni and Cu had a normalized concentration distribution similar to bromide, except that Ni and Cu transport were retarded in the pristine zone. Normalized Cr concentrations were less than those of Br and Ni below the oxic/suboxic boundary (Figure 7 and 8), but dissolved Cr was present as far back as the injection MLS in the pristine zone (Figure 8).

The pattern for dissolved Zn deviated from the other tracers, especially within the Zn-contaminated region of the aquifer. Above and below the region, the 0.002 concentration contour represents Zn added by the tracer test to the pristine and sewage-contaminated zones. Zn transport was retarded in the pristine zone, with tailing similar to that observed for Ni and Cu (Figure 7). The pre-existing Zn contamination (the extent of which is shown in gray in Figures 7 and 8) makes closure of the outermost 0.002 contour uncertain within the Zn-contaminated region. Inside the Zn-contaminated region, and early in the tracer test, the highest Zn concentration contour was 1.0, five times greater than the highest contour of the other injected tracers (Figure 7) and the highest Zn concentrations were distributed along the base of the Zn-contaminated region (Figure 8). Thus, there was a large, localized increase in dissolved Zn within the tracer cloud at the bottom of the Zn-contaminated region, where the highest pre-injection dissolved Zn concentrations (>4 micromolar) were measured (Figure 4).

Figures 7 and 8 also include concentration contours for dissolved Fe and Al at 13 days, and Fe at 83 days. Thirteen days after the injection, the outer contours of both the Al and Fe clouds were similar, and the highest concentrations of both elements were found in the upper portion of the aquifer (the pristine zone). Most of the Al mass was concentrated at altitudes in the pristine zone, whereas high concentrations of Fe (> 20 micromolar) were measured at lower altitudes in the Zn-contaminated region and sewage-contaminated zones (Figure 7). These elements were not added as tracers to the injected groundwater and were therefore evidence for the occurrence of metal exchange and mineral dissolution reactions. The accumulation of aluminum in the tracer cloud appears to be the result of an intermediate reaction; it was absent from the tracer cloud by Day 83. Iron continued to accumulate in the tracer cloud at all depths and the distribution of Fe was nearly as extensive as Ni and Br after 83 days (Figure 8).

Examples of breakthrough curves from various altitudes at each MLS are shown in Figures 9 and 10. In agreement with the synoptic data discussed above, Fe was measured at BT1 and BT2, while Al was only measured at BT1 (Table 1, data not plotted). No Pb was measured at either breakthrough MLS; the data shown in Figure 8 are from MLS just west of BT1.

As altitude decreased, the reactive tracer peaks appeared closer to, but always after, the bromide peaks. Metal-EDTA complexes are known to adsorb on Fe and Al oxyhydroxide minerals (Bowers and Huang, 1986; Bryce et al., 1994; Nowack and Sigg, 1996; Nowack et al., 1996) that coat the aquifer sediments (Coston et al., 1995). The peaks of all the injected metal-EDTA complexes and chromate were retarded to the greatest degree in the pristine zone (Figures 9a, 10a). The anionic complexes were expected to adsorb more as pH decreased, consistent with the ligand-like adsorption proposed by Benjamin and Leckie (1981). Breakthrough curves in the pristine zone had long trailing limbs, an observation that is consistent with the long, drawn out tails of longitudinal contours in the pristine zone (Figure 8) and significant retardation.

The shapes of breakthrough curves at altitudes below the pristine zone generally resembled Br curves from the same depth; they were more symmetric and had narrower peak widths (Figures 9b-e and 10b-e). At the lower altitudes, reactive tracers peaked within a day or two after bromide, indicating decreased retardation of the reactive tracers. In the portion of the aquifer where the tracer test was conducted, pH and altitude were negatively correlated; the pH of groundwater in the sewage-contaminated zone was greater than 6.0 (Figure 4). Also, the concentration of competing anions (e.g., phosphate) increased (Davis et al., 2000a). Both the higher groundwater pH and phosphate caused weaker adsorption of the anionic tracers. Thus, the more compact shape of the tracer cloud in the sewage-contaminated zone reflects the influence of decreased retardation.

A complex breakthrough pattern emerged for Zn in the Zn-contaminated region (Figures 9b,c and 10b,c). Speciation data indicated a peak in dissolved Zn^{2+} concentration that appeared consistently before the peak for Zn-$EDTA^{2-}$. The size of both the total Zn peak and the Zn-EDTA peaks exceeded bromide, indicating addition of dissolved Zn mass to the tracer cloud in this region. In contrast to all the other tracers, Zn mass was present as both a cation (Zn^{2+}) and anion (Zn-$EDTA^{2-}$). The ionic strength of the tracer cloud was greater than that of the ambient groundwater, and as the tracer cloud advanced, equilibration of the porous medium with the higher ionic strength water of the cloud caused a slight decrease in pH (Davis et al., 2000a). The decrease in pH and the higher ionic strength may each have contributed to the small peaks in Zn^{2+}.

Chromium Transport

Figure 11 shows dissolved Cr mass (normalized to initial Cr mass and relative to normalized Br mass) plotted for each synoptic sampling round. Dissolved Cr decreased to about 50% of the injected Cr mass over the first 100 days after injection, and continued to decline at a slower rate over the remainder of the test. The distributions illustrated in the

longitudinal cross sections suggest that more Cr mass (i.e., C/C_o contours > 0.2) was in the upper portion of the tracer cloud, above the oxic/suboxic boundary (Figures 7 and 8).

Attenuation of Cr was evident from the reduction in area under the breakthrough curves relative to Br curves. For example, at BT1 in the pristine zone, the ratio of Cr to Br was 2.8 (Table 1), and decreased to a ratio slightly less than 1.0 at 12.1 meters, that is, where the chemical gradients in DO, pH, and competing anions began (Figure 2). Farther downgradient at BT2, Cr persisted at the intermediate elevations of the transitional zone. Cr was nearly completely partitioned to the sediments at lower altitudes at BT1 and BT2. Retardation of Cr(VI) in the pristine zone was similar to that observed for the metal-EDTA anionic complexes (Tables 3 and 4) and was at or near 1.0 in the Zn-contaminated region and sewage-contaminated zone (Figure 12).

Cr(VI) transport through the aquifer was affected by two major chemical processes: 1) reversible adsorption of Cr (VI), and 2) reduction to Cr(III) (Figure 13). The influence of these processes on Cr(VI) transport at this field site was investigated in an earlier series of small-scale tracer tests at the field site. Two kilometers downgradient of the large-scale tracer injection, Cr(VI) transport was controlled by weak, reversible adsorption in the pristine zone (Kent et al., 1995). In a tracer test conducted in the suboxic region, Cr(VI) adsorption was very weak due to the higher pH and the presence of competing anions, and little retardation was observed (Kent et al., 1994; Friedly et al., 1995). The adsorption of competing anions has also been shown to influence the pH dependence of molybdate adsorption on aquifer sediments at this site (Stollenwerk, 1995). Reduction from Cr(VI) to Cr(III) occurs under suboxic conditions, and Cr(III) is so strongly adsorbed that it can be considered immobile (Anderson et al., 1994).

Effect of Metal Exchange Reactions on Lead and Copper Transport

Adsorbed metal-EDTA complexes may undergo metal exchange reactions in which one metal is replaced by another in the complex, including reactions where Fe(III) dissolves from an Fe oxide and exchanges with a metal complexed by EDTA (Nowack and Sigg, 1997). Column and batch experiments with pure mineral phases and natural sediments have shown that metal-EDTA complexes can react with hydrous oxides to form dissolved Al- or Fe-EDTA complexes (Bowers and Huang, 1987; Davis et al., 1993b; Girvin et al., 1993; Bryce et al. 1994; Brooks, et al. 1996; Nowack and Sigg, 1997).

The overall transport of the metal-EDTA complexes can be qualitatively explained by comparing the zeroth moment (calculated from the synoptic datasets, see Davis et al., 2000a) for each metal (Figure 14). Although EDTA was not measured in all synoptic samples, the sum of the dissolved metals, Al, Cu, Fe, Ni, Pb, and Zn, was very well correlated (R^2=0.985) with the EDTA concentrations measured in the temporal and transect samplings (Davis et al., 2000a).

Metal exchange reactions explain the appearance of dissolved Fe and Al within the EDTA tracer cloud, where the Fe and Al were primarily derived from the dissolution of oxide coatings on the sediment grains in the aquifer, e.g., for Fe:

$$MeEDTA^{2-} + Fe(OH)_{3,s} + >SOH + 2H^+ = FeEDTA^- + >SOMe^+ + 3H_2O \quad (1)$$

where Me is Pb, Cu, Ni, or Zn. Measurable concentrations of Al and Fe were dissolved from the sediments within the first 24 hours after the injection (Figure 15). During the first two days of the tracer test, dissolved Al concentrations were greater than Fe, and the Al concentrations were inversely correlated with pH (Figure 15). The appearance of dissolved Al in the EDTA tracer cloud was short-lived (Figure 14) and most of the Al mass appeared in the pristine zone and at the top of the Zn-contaminated region (Figure 7). Although Fe^{3+} forms a stronger complex than Al^{3+} with EDTA, the formation of Fe(III)-EDTA complexes apparently was limited by reaction kinetics initially. The Fe(III)- and Al-EDTA complexes were less retarded during transport than the reactive tracers whether calculated by the temporal or spatial moment data sets (Synoptic R_f of Al = Fe = 1.10; for breakthrough MLS see Tables 3 and 4).

The mass of dissolved Fe in the EDTA tracer cloud increased over the entire experiment (Figure 14). At chemical equilibrium, the degree of exchange of the four injected metals with Fe(III) via the reaction shown in Equation 1 is different for each metal and is dependent on pH, the concentration of the metal-EDTA complexes, and other chemical factors. An important consideration was that, for a given set of conditions in the aquifer, the exchange reaction becomes more favorable with a decrease in the concentration of metal-EDTA complexes. Thus, dilution of the tracer cloud by dispersion enhances the exchange reaction with Fe(III) to form Fe(III)-EDTA.

Transport of Pb was attenuated sharply and dissolved Pb never reached BT1 or BT2 in detectable concentrations. The retardation factor for Pb, estimated from the synoptic data, was 1.28. Dissolved Pb disappeared from the tracer cloud completely within 111 days. Data collected during the first seven days of the tracer test along a longitudinal transect show that significant Pb metal exchange occurred after injection (Figure 16a). If no metal exchange had occurred, *i.e.* if $Pb\text{-}EDTA^{2-}$ and $Cu\text{-}EDTA^{2-}$ complexes behaved like $Ni\text{-}EDTA^{2-}$ complexes, then all the data shown in Figure 16a should collapse to a value of 1.0 on each axis, as the $Cu\text{-}EDTA^{2-}$ data does. There was a correspondence between the loss of dissolved Pb and the addition of dissolved Zn, as $Zn\text{-}EDTA^{2-}$, within the Zn-contaminated region of the aquifer (Figure 16b). Pristine zone samples also had the highest concentrations of Fe- and Al-EDTA complexes during the first 7 days after injection (Figure 16c). These data indicate the decrease in dissolved Pb was enhanced under pristine and Zn-contaminated conditions, which is consistent with observations of dissolved Pb in the synoptic data (Figures 7 and 8).

Cu-EDTA exchange for Zn^{2+} within the Zn-contaminated region of the sewage- contaminated zone probably occurred during the tracer test (note the break in the 0.1 contour for Cu in Figure 8), but was not significant during the first 7 days after injection (Figure 16a). Later in the test, the temporal moments calculated from BT1 and BT2 showed significant attenuation occurred over the entire region (Table 1 and 2). The calculated retardation factors were highest in the pristine zone and approached 1.0 at sampling ports within the sewage-contaminated zone (Table 3 and 4). However the overall retardation, as calculated from the zeroth moments, was 1.24, 4% greater than calculated for Ni.

Cu^{2+} and Pb^{2+} formed by metal-exchange reactions (Equation 1) would be strongly adsorbed by the porous medium; thus, the result of the metal exchange process was a decrease in the dissolved masses of Cu and Pb. In contrast, Ni-EDTA complexes did not appear to undergo significant metal exchange; the main reaction that affected Ni transport was adsorption of the Ni-EDTA complexes (Davis et al., 2000a,b). The transported mass of Ni remained essentially constant throughout the tracer test, while the masses of Pb and Cu decreased significantly (Figures 14 and 17).

Zinc Transport

The effect of the pre-injection Zn^{2+} contamination in the aquifer on the transport of the metal-EDTA complexes was significant. Dissolved Zn mass increased over the first 83 days of the experiment, was approximately constant for the next 100 days, and then decreased after 175 days (Figure 14). At the plateau, the mass of dissolved Zn was greater than the mass of Ni by a factor of 1.6 to 1.8. The increase in Zn mass must be due to exchange reactions between the metal-EDTA complexes and the adsorbed Zn in the Zn-contaminated region (Figure 4). For the first 175 days (and 71 m) of transport, the center of mass for Ni remained in the Zn-contaminated region (Davis et al., 2000a). Outside of the Zn-contaminated region, dissolved Zn was missing where Ni and Fe were still present (Figure 8). Thus, during transport, Zn mass was lost from the portion of the tracer cloud outside the Zn-contaminated region, but there was a concurrent increase in Zn mass within this region.

Analysis of the Zn speciation data collected at BT1 and BT2 suggests the processes by which Zn mass increased during transport. The injection was designed such that the tracers were injected across vertical gradients in dissolved and adsorbed Zn. In addition, the tracer cloud was transported horizontally through and out of the Zn-contaminated region; thus, there were also horizontal gradients in Zn^{2+} (Figure 4). Zn_T/Br and Zn_{free}/Br breakthrough curve area ratios exhibit different trends in comparison to the other tracers (Tables 1 and 2), where Zn_T refers to the total dissolved Zn concentration and Zn_{free} refers to that portion not complexed with EDTA . The calculated ratios for Zn_T/Br were as large as 3 at the Zn-contaminated region altitudes and were consistent with a net increase in dissolved Zn mass along the sampled flow paths. The largest increase in Zn concentrations occurred at the same altitudes with lower Cu/Br and Fe/Br breakthrough curve area ratios and near the bottom of the Zn-contaminated region. This observation, along with the earlier observations regarding Pb transport in the Zn region, suggested that Zn and Fe were competing as reactants in metal exchange reactions with Cu- and Pb-EDTA complexes.

Reactions that could have increased the dissolved Zn mass in the Zn-contaminated region and early in the tracer test include the following:

$$>SOZn^{+} + CaEDTA^{2-} + H^{+} = >SOH + ZnEDTA^{2-} + Ca^{2+} \quad (2)$$

$$>SOZn^{+} + PbEDTA^{2-} = >SOPb^{+} + ZnEDTA^{2-} \quad (3)$$

$$>SOZn^{+} + CuEDTA^{2-} = >SOCu^{+} + ZnEDTA^{2-} \quad (4)$$

where >SOH represents a generic sorption site. The reaction in Equation 2 represents the desorption of Zn from aquifer sediments in the Zn-contaminated region by the slight EDTA excess in the injectate (shown here as complexed with Ca, but some was complexed with Mg and Al). Equation 2 would have contributed to increased Zn mass only until Zn had displaced Ca and other weakly bound cations from the small amount of excess EDTA, a process that was complete within the first 13 days of the tracer test. Increases in dissolved Zn due to Equation 2 have been observed in small-scale tracer tests (Kent et al., 1992). The influence of Equations 3 and 4 on dissolved Zn is apparent in the longitudinal sections through the tracer cloud 13 days after injection, where normalized Zn concentrations greater than 1 can be seen (Figure 7).

The effect of the background dissolved Zn^{2+} on the zeroth moment for Zn has not been quantified. The injectate solution initially had 266 μM dissolved Zn as Zn-$EDTA^{2-}$ complexes (Davis et al., 2000a,b). Increases in dissolved Zn mass could occur as the equilibrium between adsorbed and dissolved Zn was reestablished; the magnitude of this process would depend upon the rate at which adsorption equilibrium was reestablished in comparison to the rate of movement of the tracer cloud. All breakthrough curves from altitudes within the Zn-contaminated region (Figures 9b,c and 10b,c) had measurable concentrations of Zn_{free} during the period that the EDTA tracer cloud passed, suggesting that Zn desorption was increasing the Zn^{2+} concentration back towards its equilibrium value on the time-scale of transport. However, the pH also decreased slightly at the leading edge of the tracer cloud, and this probably caused some additional desorption of Zn^{2+}.

Dissolved Zn mass continued to increase slowly after 48 days (Figure 18), primarily due to the reaction in Equation 4. Cu concentrations were very small in comparison to Ni concentrations within the Zn-contaminated region at 175 days (Figure 19). By 237 days, relative Cu concentrations (C/C_o) were less than 0.1, while relative Ni concentrations greater than 0.1 still occurred in the Zn-contaminated region. Because of the low Cu concentrations in the Zn-contaminated region and a continual increase in the fraction of the tracer cloud that traveled outside of this region, the contributions to dissolved Zn mass by Equation 4 were too small after 175 days to offset the loss of dissolved Zn by Zn-EDTA exchange with Fe(III). Therefore, the net result became negative, and dissolved Zn mass decreased substantially in subsequent synoptic samplings (Figure 18).

Laboratory Studies of the Dissolution of Iron and Aluminum from Aquifer Sediments by EDTA

Rates of mineral dissolution are known to depend on pH, ionic strength, ligand concentration, and the number of ligand functional groups coordinated to the surface. Al oxide and oxyhydroxide solubilities are strongly influenced by pH; however, in natural systems, dissolved silica, phosphate, and sulfate also affect Al solubility (Lindsay and Walthall, 1995). The aquifer sediments at the study site are coated with an assemblage of Al-, Fe-, and Si-bearing minerals (Coston et al., 1995; Fuller et al., 1996), and the surface mineralogy may be altered in the sewage-contaminated zone by the presence of various solutes (Mn, phosphate, sulfate) and higher pH. Because the dissolution rates of Fe and Al are so critical to the fate of metal-EDTA complexes in the aquifer, a separate study of these rates in batch experiments was undertaken.

The results suggest that numerous factors influenced the rates of metal exchange reactions with Fe and Al during the field experiment. Figure 20 shows the concentrations of Fe, Al, and EDTA present in batch experiments conducted under two sets of experimental conditions: 1) “pristine”, using sediments from the pristine zone and artificial groundwater at pH 5.4, with major ion composition similar to that of the pristine zone of the aquifer; and 2) “sewage-contaminated,” using sediments from the sewage-contaminated zone and artificial groundwater at pH 6.5, with major ion composition similar to that of the sewage-contaminated zone of the aquifer. Fe dissolution was slower than Al under pristine zone conditions, but Fe dissolution continued slowly throughout the 14 day reaction period. The concentration of Al-EDTA complexes peaked during the kinetic experiments (at 4 hours, pristine; at 48 hours, sewage-contaminated), and based on mass balance considerations, the subsequent dissolution of Fe must have involved an Al-Fe exchange reaction with $AlEDTA^-$ species.

Iron extracted by a 0.5 hour hydroxylamine-HCl (HH) extraction is presumed to represent an estimate of the amount of amorphous iron oxyhydroxides in the sediment (Chao and Zhou, 1983). The amounts of Fe and Al dissolved by the HH extraction were determined for each of the sediment composites. The extraction results were normalized by surface area and compared with the apparent dissolution rates of Fe and Al determined from the EDTA batch experiments (Table 5). The apparent dissolution rates were calculated based on linear regressions of portions of the curves shown in Figure 20. In addition to the oxic and sewage-contaminated zone experiments, the results of EDTA batch experiments with the Zn-contaminated composite sample from the Zn-contaminated region are shown in Table 5. The dissolution “rates” shown are the net result of several different simultaneous reactions and should not be extrapolated to other conditions, as the mass distribution between metal-EDTA complexes on the surface was not known, and the values shown were solely based on the appearance of Fe- or Al-EDTA complexes in solution.

The pristine and sewage-contaminated composites contained similar amounts of HH-extractable Fe, but the Zn-contaminated composite from the Zn-contaminated region had nearly twice the mass of amorphous Fe (Table 5). Thus, the fast initial rate of Fe dissolution by EDTA from the Zn-contaminated composite may be due to a larger amount of amorphous Fe material present. The rate of Fe dissolution from iron oxides by EDTA increases with increasing pH (Chang and Matijevic, 1983; Nowack and Sigg, 1997), and the difference between the pristine and sewage-contaminated composites which had similar amounts of amorphous Fe was consistent with the pH dependence of the reaction rate. These observations suggested that exchange and dissolution reactions with the metal-EDTA complexes (i.e., Equation 1) were affected by a spatial variability in the abundance of amorphous Fe oxyhydroxide in the aquifer as well as the pH gradient.

The rate of iron dissolution by EDTA is also known to be dependent on the crystallinity of iron oxide phases (Borggaard, 1976; Borggaard, 1991; Nowack and Sigg, 1997). For example, EDTA dissolution of pure ferrihydrite in the laboratory is rapid (Rea et al., 1994) and much faster than observed for crystalline iron oxides. However, in natural sediments the rate of Fe dissolution of poorly crystalline Fe phases by EDTA may be quite slow (Borggaard, 1976; 1979). The difference between dissolution rates with pure mineral phases and natural sediments is probably due to the formation of other competing metal-EDTA complexes, and also the presence of competing anions, such as PO_4 (Borggaard, 1991) or silicate (Zachara et al., 1995a) at the mineral surface.

While several studies have been published on the dissolution of Fe oxides by EDTA and metal-EDTA complexes, the dissolution of Al oxides has not been well studied. Girvin et al. (1993) measured the concentration of dissolved Al in their

experimental system (Co(II,III)-EDTA and γ-Al_2O_3) and found that Al-EDTA complexes dominated the solution speciation below pH 6.5 but were not the dominant adsorbing species. However, the amount of Al dissolved did not exhibit a consistent trend with respect to either variable metal-EDTA complex concentration or γ-Al_2O_3/water ratio, and the concentration of dissolved Al was approximated based on a fit to experimental data rather than a particular mineral solubility, such as gibbsite. In another study, although metal-EDTA complex dissociation was observed in the presence of γ-$Al_2O_{3,}$ Bowers and Huang (1986, 1987) did not report whether Al-EDTA complexes were formed.

The slower rate of Al dissolution at the higher pH in the sewage-contaminated experiments (Figure 20) is consistent with other work on EDTA dissolution of natural sediments at neutral pH (Aggett and Roberts, 1986). Al dissolution in the sewage-contaminated zone experiments had both fast and slow processes which was not apparent in the experiments conducted under pristine and Zn-contaminated conditions. There may have been a difference in the surface mineralogy of the sewage-contaminated composite or possibly, as has been found for Fe, adsorbed phosphate or silicate also interfered with the dissolution of Al. The high intercept value for Al dissolution under pristine zone conditions suggested that the lower pH enhanced the solubility of aluminum minerals in the sediment. Nonetheless, these results were consistent with the tracer test observations, that is the initial formation of Al-EDTA complexes was correlated with lower pH values (Figure 15), and significant dissolved Al mass was observed only during the beginning of the tracer test (Figure 14).

The computed intercept of Zn extracted by EDTA from the Zn-contaminated sediments was more than the Zn mass extracted by the hydroxylamine-HCl extraction (Table 5). HH-extractable Zn may be an underestimate of the Zn mass capable of forming EDTA complexes in the aquifer. As suggested by Equation 2, a portion of the injected free EDTA was probably complexed with both Zn and Al in the Zn-contaminated region. Preliminary data from experiments in which artificial groundwater containing Pb-EDTA complexes was equilibrated with Zn-contaminated aquifer sediments indicated that metal exchange reactions involving Pb and Zn as described by Equation 3 can also occur.

In the batch experiments (Figure 20), the concentrations of Fe-EDTA complexes continued to increase slowly over time, suggesting that the process of Fe dissolution and metal exchange was rate-controlled by one or a series of reactions. This behavior has been observed in other multicomponent systems (Yu and Klarup, 1993). Nowack and Sigg (1997) demonstrated that rates of Fe dissolution were slower when EDTA was added as a metal complex (such as Al-, Zn-, or Ni-EDTA), and the effect was more pronounced with poorly crystalline oxyhydroxide phases. It is also important to consider how the formation and subsequent readsorption of Al–EDTA complexes (and in the Zn-contaminated region, Zn-EDTA complexes) may effect changes in the observed rate of Fe dissolution. Bowers and Huang (1987) showed that the addition of Zn- and Fe-EDTA complexes to a suspension of γ-Al_2O_3 resulted in dissociation of the Zn-EDTA complex and formation of Fe-EDTA complexes at pH values less than 7.0. Hence, the rates reported in Table 5 represent maximum dissolution rates, as it is expected that the addition of EDTA as a metal-EDTA complex would cause the rates of dissolution to decrease.

Implications for Reactive Transport Modeling

A principal objective of this tracer test was to create a data set that would stimulate the testing and development of predictive models of reactive contaminant transport. Data sets generated from field studies are often too poorly constrained with respect to source terms, boundary conditions, and available data to provide rigorous testing of reactive transport modeling approaches. Most field and laboratory experimental studies of reactive solute transport have been conducted under relatively uniform chemical conditions, that, although well-constrained, may not offer challenges to reactive transport modeling approaches that are sufficiently rigorous. This tracer test was designed such that chemical conditions in the aquifer varied over the spatial domain of the tracer test.

Spatial variability in groundwater chemistry was mostly provided by the vertical gradients across which the tracer cloud was injected. Vertical gradients in pH and concentrations of anions (Kent et al., 1994) affected the adsorption, and therefore the retardation of Cr(VI) and each of the metal-EDTA complexes. Vertical gradients in redox conditions resulted in changes in the reduction of Cr(VI) with depth. The gradients in pH also affected the displacement of Cu, Zn, and Pb from EDTA complexes by controlling the solubility of hydrous ferric oxides. In addition to the variations in groundwater chemistry, the Zn-contaminated region was a distinctive feature of vertical and horizontal variability in chemical properties of the porous medium. Both the thickness and extent of Zn-contamination varied along the path of the tracer cloud.

A large network of chemical equations must be solved in reactive transport simulations of this tracer test because of the number of reactants and products. Considering both the tracers and the chemical constituents of the aquifer, there are at least 185 solution species, 66 solid phases, and 46 adsorbed species that could be considered in transport modeling. However, it is possible to simplify the problem by eliminating those reactions and chemical species that do not have a

significant effect on the modeling result. For example, by eliminating species that affected either the activity or total dissolved concentration of a tracer by less than 1% in the batch geochemical model, HYDRAQL (Papelis et al., 1988), the chemical problem could be simplified to one with 54 solution species, 3 solid phases, and 38 adsorbed species (Davis et al., 1993a). Whether the 1% criterion is appropriate or, perhaps, too restrictive for transport modeling will require further study.

The modeling investigations conducted by our group and collaborators to date have focused on 3 sets of chemical processes that have been simulated independently from one another. The first modeling study addressed the influence of redox reactions on Cr(VI) transport. The second study illustrates some of the principal factors that influenced the extent of metal exchange reactions of the EDTA complexes. The third study demonstrates a viable approach for modeling the influence of adsorption on transport under variable chemical conditions.

Modeling the Transport of Cr(VI)

Analysis of the results of small-scale tracer tests showed that the observed loss of Cr(VI) in the suboxic zone resulted from rate-limited reduction of Cr(VI) to Cr(III), which was immobilized on the sediments (Kent et al., 1994). Fe(II)-bearing minerals in the porous medium were the principal reductants (Anderson et al., 1994). The rate of Cr(VI) reduction observed in well-stirred batch reactors, which was limited by diffusion into the sediment grains, had a time-scale of the order of 1-2 days (Anderson et al., 1994). The rate of reduction observed during the field experiments, however, was significantly slower, with a time-scale on the order of 10 days. Model simulations of both laboratory and field experimental data led to the conclusion that Cr(VI) reduction during transport was limited by the rate of mass transfer to the surfaces of the reductant mineral phases. On average, the rate of Cr(VI) reduction in the field could be simulated by the rate of diffusion out of a nonreductive sediment layer approximately 22 cm thick to a thin layer (2.4 cm thick) containing the reductant minerals (Friedly et al., 1995). Depositional features of thin strata with large abundances of heavy minerals at this scale have been observed at the field site (Barber, 1990; Hess et al., 1992; LeBlanc et al., 1991).

Differences between the results of the large-scale test reported herein and the previous small-scale experiments will provide a basis for testing the extrapolation of such modeling approaches to large-scale contaminant transport applications. One difference is the higher initial concentration of Cr(VI) used in the large-scale experiment (506 μM) in comparison to 100 μM used in the small-scale experiments. In the small-scale field experiments, there was a five-fold excess of reductive capacity in the porous medium compared with the moles of Cr(VI) injected, even without considering transport. In the large-scale test, the moles of Cr(VI) injected were roughly equivalent to the reductive capacity of the porous medium initially contacted by the groundwater with tracers. In the transport model (Friedly et al., 1995), a rate expression that was first order with respect to Cr(VI) concentration was used to describe the mass-transfer rate into the sediment layers containing the reductant. In accordance with this model, the initial rate of Cr(VI) mass transfer and reduction should have been much faster during the large-scale test, and Cr(VI) should not have traveled much farther downgradient in the suboxic zone than was observed in the small-scale tracer tests. Differences in scale between this experiment and the small-scale tests also mean that contact times of aquifer sediments with the tracers were greater in the large-scale tracer test because of the length of the tracer cloud.

The fact that the tracer cloud was injected across the pristine, Zn-contaminated region, and sewage-contaminated zones adds additional challenges to modeling Cr(VI) reduction during transport. Whether Cr(VI) reduction could occur to a measurable extent in the pristine zone is unknown. Small-scale tracer tests conducted in pristine groundwater at a site approximately 2 km downgradient showed no evidence of reduction over the short (2 m) transport distance observed (Kent et al., 1995). However, the large-scale tracer test was carried out much closer to the effluent disposal beds where redox conditions likely fluctuated historically in response to changes in the quantity and quality of the sewage effluent. Indeed, Cr(VI) reduction occurred in the suboxic zone even in the presence of dissolved oxygen concentrations high enough to make Cr(VI) the thermodynamically stable species (Kent et al., 1994). Prolonged exposure to oxygen in the vadose zone deactivates the Cr(VI)-reductive capabilities of Fe(II)-containing minerals (White and Peterson, 1996), and sediments in the pristine zone may have been unsaturated during periods of low recharge. Whether or not Cr(VI) reduction occurred in the oxic zone, it is likely that the reductive capacity varied with depth through the Zn-contaminated region (Figure 13). Moment computations for both Br and Ni show that an increasing fraction of the tracer cloud moved from the oxic zone into the Zn-contaminated region and sewage-contaminated zone during the tracer test (Davis et al., 2000a,b). Thus, a significant vertical flux of Cr(VI) from the oxic into the Zn-contaminated region and suboxic zones will have to be accounted for in simulations of Cr(VI) reduction during transport.

Adsorption was also considered in modeling the fate and transport of Cr(VI) in the suboxic zone during small-scale tracer tests (Friedly et al., 1995). In modeling retardation of Cr(VI) in the suboxic zone, where chemical conditions were constant, Friedly et al. (1995) used a simple reaction of the form:

$$>S + Cr(VI) = >SCr(VI) \quad (5)$$

in which >S represents an adsorption site and Cr(VI) represents the total dissolved Cr(VI) concentration. The stability constant for this reaction was fit to the Cr(VI) retardation observed in the experiment. This simplified approach cannot

be used in the large-scale tracer test because of the vertical gradient in groundwater chemistry in the region into which the tracer cloud was injected. The gradient in pH and the increase in PO_4 and other anion concentrations, resulted in weaker Cr(VI) adsorption and less retardation in the suboxic zone (Figure 12). Kent et al. (1995) developed a model to account for Cr(VI) adsorption in the pristine zone as a function of pH and sulfate concentration, however, reactions for phosphate adsorption should also be included (Kent et al., 1994). Stollenwerk (1995) successfully described molybdate adsorption onto Cape Cod sediments solids over a similar range of chemical conditions with variable phosphate. In that study, the set of parameters that fit batch adsorption data also described the main features of molybdate transport in column experiments conducted over a range of chemical conditions. Adsorption reactions for the metal-EDTA complexes will also be required to account for differences in the retardation of metal-EDTA complexes observed at different altitudes in the aquifer. Competitive adsorption of the metal-EDTA complexes may also have influenced Cr(VI) adsorption.

Modeling Metal Exchange Reactions of Metal-EDTA Complexes

Dissolved Pb, Cu, and Zn were lost or gained within regions of the aquifer as the tracer cloud moved downgradient. The observed losses in dissolved metals resulted from displacement of the metals from EDTA complexes by Fe(III) or Al dissolved or Zn desorbed from the aquifer sediments. In the regions of the aquifer without Zn contamination, the observed rate of metal exchange decreased in the order Pb>>Zn>Cu. There was no evidence that a significant mass of Ni was lost from the tracer cloud (Davis et al., 2000a,b).

Understanding the overall result of the metal exchange reactions requires a consideration of complexation, dissolution, and adsorption reactions. The reactions can be written as follows:

$$MeEDTA^{2-} + Fe(OH)_{3,s} + 3H^{+} = FeEDTA^{-} + Me^{2+} + 3H_2O \quad (6)$$

$$Me^{2+} + >SO_sH = >SO_sMe^{+} + H^{+} \quad (7)$$

where Me represents Pb, Zn, Cu, or Ni, and $>SO_sH$ represents a strong-binding surface site available for adsorption of the metal ions. The aqueous complexation and Fe(III)-oxyhydroxide dissolution reactions are combined in Equation 6. Using a solubility product of –38.8 for $Fe(OH)_{3,s}$ (Morel and Hering, 1993) and the aqueous complexation constants of Martell and Smith (1989) for metal-EDTA complexes, the apparent thermodynamic affinity for the metal exchange Equation 6 increases in the order Zn>>Pb>Ni>Cu (Table 6). In other words, if adsorption (Equation 7) of the metals is unimportant, then the thermodynamic constants lead to the conclusion that $ZnEDTA^{2-}$ should be affected by the metal exchange reaction the most, followed by $PbEDTA^{2-}$, $NiEDTA^{2-}$, and then $CuEDTA^{2-}$. The values of stability constants for adsorption reactions on the Cape Cod aquifer sediments, represented by Equation 7, are only known well for Zn^{2+} at this point in time (Davis et al., 1998). However, it is believed that the stability constants for Equation 7 also influence the order of the metal exchange reactions observed in the field. To illustrate this point, consider the stability constants (Table 7) for adsorption of the metal ions onto the surface of the poorly crystalline mineral, ferrihydrite, a commonly found Fe oxyhydroxide coating on sediment surfaces, tabulated from Dzombak and Morel (1990). The constants in Table 7 can only be applied consistently when used with the two-site diffuse double layer surface complexation model of Dzombak and Morel (1990) and the surface density value of strong-sites that those authors chose. The constants illustrate that the strength of the adsorption reactions increase in the order Pb>>Cu>>Zn>Ni. Thus, Pb^{2+} adsorbs at a lower pH value on ferrihydrite than the other metal ions. This general preference among the metal ions for adsorption on oxide surfaces is likely true for the Cape Cod sediments, although the thermodynamic preference for Al oxide coatings may be somewhat different (Coston et al., 1995). In addition, the proton stoichiometry of the reactions and electrical double layer corrections in the mass law may differ (Davis et al., 1998). By combining Equations 6 and 7, one obtains the following reaction:

$$MeEDTA^{2-} + Fe(OH)_{3,s} + >SO_sH + 2H^{+} = FeEDTA^{-} + >SO_sMe^{+} + 3H_2O \quad (8)$$

The stability constants of Equation 8 can be determined as the product of the constants for the reactions in Equations 6 and 7. Using ferrihydrite as an analogue for the Cape Cod sediment (Equation 8), one obtains the stability constants shown in Table 8. With the two reactions combined, one obtains the same order in affinity of metal exchange as was observed in the tracer test (outside of the Zn-contaminated region): Pb>>Zn>Cu>>Ni. Thus, it appears likely that the adsorption reactions were critical components of the reaction network affecting the transport of Pb, Zn, Cu, and Ni during the tracer test.

An equilibrium chemical model was developed to illustrate how these reactions may have controlled the evolution of the loss of dissolved Pb, Zn, Cu, and Ni from the tracer cloud. The equilibrium model included both the strong- and weak-site adsorption reactions of the four metal ions on the Cape Cod sediment, assuming that the stability constants were the same as those in Dzombak and Morel (1990). Site density was estimated from the specific surface area of the sediment (0.44 m^2/g), an assumed value of 3.84 mmoles sites/m^2 of surface area (Davis and Kent, 1990), also used by Dzombak and Morel (1990), and the aquifer porosity (0.39, equivalent to 4.14 kg sediment/L of water). Adsorption constants for the metal-EDTA complexes, including Fe(III), were included in the model, and these constants were estimated from the

retardation of metal-EDTA complex transport in the pristine zone of the aquifer. The model calculations were performed assuming that the background chemistry was similar to that found in the sewage-contaminated zone outside of the Zn-contaminated region.

Figure 21 shows the calculated equilibrium concentration of Fe(III)-EDTA complexes that would be dissolved in the aquifer as a function of pH after reaction with groundwater containing 250 μM of one of the four injected metal-EDTA complexes. Note that the model predicts that the favored metal exchange reaction with Fe(III) is that of the Pb-EDTA complexes, which are predicted to proceed to near complete exchange for pH values less than 6. Zn-EDTA complexes are predicted to be the next to exchange with Fe(III), but only slightly in the pH range 6.0-6.5. Cu-EDTA complexes begin exchanging at higher pH values than Ni-EDTA complexes. The Cu-EDTA exchange with Fe(III) has a different slope as a function of pH than the other 3 metals; the reason for this is that the calculated Cu-Fe exchange occurs in the same pH range as the Cu adsorption edge on the Cape Cod sand. For the other 3 metals, the pH regions for the adsorption edge and exchange with Fe(III) did not overlap significantly.

In addition to pH, the amount of Fe(III) dissolved at equilibrium is sensitive to the concentration of metal-EDTA complexes. For example, Figure 22 illustrates the calculated percent of EDTA present as dissolved Ni-EDTA complexes in the aquifer as a function of pH and the total concentration of Ni-EDTA complexes added to the groundwater. As the concentration of Ni-EDTA complexes decreases, the metal exchange reaction with Fe(III) is more favored, and thus significant Ni-Fe exchange could occur at pH 6 once the tracer cloud was diluted by factors greater than 1000. While it was possible that dissolution and metal exchange reactions occurred with the Ni-EDTA complexes, we could not quantify a loss of Ni mass in the field data set (Davis et al., 2000a,b).

The calculations above are meant to illustrate qualitatively that the observed order of metal exchange in the field experiment may be consistent with the overall thermodynamics of the system. However, the calculations cannot be considered quantitative because of several major uncertainties in the thermodynamic model:

1) The stability constants used for the adsorption reactions (Equation 7) in these calculations were derived for adsorption data with pure ferrihydrite only. Different values for the metal adsorption reactions would apply for the Cape Cod sediments. An additional calculation is shown below for Zn^{2+}, for which apparent stability constants for the adsorption reactions on Cape Cod sediments have been determined.
2) The adsorption model used in the calculations included a diffuse layer electrical double layer model to correct chemical equilibria for electrostatic energy contributions at the surface. To be consistent with the constants used from Dzombak and Morel (1990), it was assumed that the electrostatic energy contribution (determined from the surface acidity constants) for the Cape Cod sediment is the same as that of the ferrihydrite surface. This is very unlikely, as the Cape Cod sediment surface should be negatively charged due to coatings, whereas the pure ferrihydrite surface would be positively charged at pH 6. Even if the chemical interactions were identical as assumed above, the metal ion adsorption on the Cape Cod sediment should be stronger than pure ferrihydrite due to a more favorable electrostatic interaction. As an aside, anion adsorption, such as that of the Cr(VI) tracer, should be weaker than that observed for pure ferrihydrite.
3) The solubility product of the Fe oxyhydroxide coatings on the Cape Cod sediment may be different than that used in the calculations.
4) The metal exchange reactions may be rate-limited in the field and may not be well described by equilibrium calculations.

For the synoptic sampling at 13 days, the highest concentrations of dissolved Fe were observed in the pristine zone (Figure 7). The highest concentration was about 50 μM at a point where the initial tracer solution was diluted in the ratio 60/40% tracer solution to ambient groundwater. Figure 23 shows the expected percentages of Pb, Zn and Cu present as EDTA complexes at equilibrium at pH 5.5 (near the values in the pristine zone). If one assumes equilibrium with respect to dissolution of ferrihydrite is attained (as in Figures 21 and 22), the dissolved Fe concentration is computed to be about 200 μM. Under these conditions, the Pb-Fe exchange is essentially complete, but the Zn-Fe exchange only occurs to a minor extent. Because significant concentrations of dissolved Al were observed (Figure 7), but are not expected at chemical equilibrium, and because the dissolved Fe observed was only 50 μM, it is likely that chemical equilibrium with the tracer cloud was limited by the rate of Fe dissolution. If the equilibrium calculation is performed such that the system is equilibrated with a dissolved Fe concentration of 50 μM, rather than equilibrium with ferrihydrite, the model predicts that Pb-Fe exchange should be about 30% complete at this point in the pristine zone (Figure 23). This is closer to what was observed at the 13 day synoptic sampling.

Thus, the metal exchange reactions of the Pb-, Zn-, and Cu-EDTA complexes during transport were probably rate-limited, although the overall order of metal exchange was likely determined by thermodynamic favorability (Table 8). The persistence of Pb-EDTA complexes in the tracer cloud suggests that the Pb-Fe exchange reaction was rate-limited. Preliminary reactive transport modeling of the results of small-scale tracer tests suggests that the Zn-Fe exchange reaction in the aquifer is limited by the rate of Fe dissolution. The results of batch experiments with the Cape Cod

sediment in our laboratory also were consistent with the hypothesis that the rates of the metal exchange reactions in the aquifer were limited by the rate of Fe(III) dissolution.

The rate-controlling step of exchange reactions of several transition metal-EDTA complexes with Fe(III) in the presence of goethite appears to be the breaking of Fe-O bonds at the mineral surface, which is independent of the particular metal-EDTA complex present (Nowack and Sigg, 1997). However, for poorly crystalline ferrihydrite, the rate of the metal exchange reaction was found to depend on the particular metal-EDTA complex present (Nowack and Sigg, 1997), suggesting the rate of free metal ion desorption also influenced the overall rate of metal exchange. Compared to the total concentration of EDTA injected (1.1 mM), an excess of poorly crystalline Fe (3.7 mmoles/liter of groundwater) was present on the aquifer sediments contacted immediately after injection, as estimated from chemical extractions (Coston et al., 1995; Fuller et al., 1996). Thus, if the conclusions of Nowack and Sigg (1997) apply in the aquifer, each individual metal-EDTA complex could have a different rate for the general rate-controlling reaction (Equation 8) involving Fe(III) dissolution and metal-EDTA exchange.

An equilibrium adsorption model for Zn^{2+} adsorption on Cape Cod sediments (Davis et al., 1998) has been developed from the results of laboratory batch experiments (Coston et al., 1995). Adsorption of Zn^{2+} was determined over the relevant ranges of pH and Zn^{2+} concentrations that exist in the aquifer. Surface complexation of Zn^{2+} with "average" surface sites on the Cape Cod sediments was described with the following two reactions:

$$>S_sOH + Zn^{2+} = >S_sOZn^{+} + H^{+} \quad (9)$$

$$>S_wOH + Zn^{2+} = >S_wOZn^{+} + H^{+} \quad (10)$$

where $>S_sOH$ and $>S_wOH$ represent high affinity (strong) and low affinity (weak) adsorption sites, respectively. No electrical double layer corrections were made to the mass laws written for these reactions. Best fits of both two-site (Equations 9 and10) and one-site (Equation 9 only) surface complexation models to the batch experimental data were determined. Fits using the two-site model were superior to those obtained with the one-site model, because of the non-linear adsorption isotherms for Zn (Figure 24). (Note: For a linear isotherm, the slope of the adsorption data should be one on the log-log plot of Figure 24). The total site density was estimated from the surface area of the sediment (as described above), and the density of $>S_sOH$ in the two-site model was determined by best fit to the data (0.86% of the total sites). Values of the stability constants for reactions in Equations 9 and 10 were log K = 0.85 and –2.40, respectively (Davis et al., 1998). Note that these constants cannot be compared directly to those of Dzombak and Morel (1990) because of the differing site densities and differing treatment of electrostatic energy terms.

The calculations presented in Figures 21-23 were made using the surface complexation constants for adsorption of metal ions on ferrihydrite (Dzombak and Morel, 1990). Figure 25 compares equilibrium calculations made with adsorption constants derived from the batch experiments with Cape Cod sediments with those of Dzombak and Morel (1990). Adsorption of Zn is stronger on the Cape Cod sediment than on ferrihydrite, and the calculations for 250 μM Zn-EDTA show that the Zn exchange reaction with Fe is more favorable at a given pH value if the stronger adsorption reactions were used in the modeling. The results show how the predicted extent of metal exchange with Fe at equilibrium depends on the values of the adsorption constants. Quantitative modeling will require that the adsorption constants for the other metal ions on Cape Cod sediments be determined, since the value for ferrihydrite appears to underestimate the strength of adsorption. Figure 25 also shows the calculated extent of Zn exchange with Fe at lower Zn-EDTA concentrations using the adsorption constants for Zn on the Cape Cod sediments. Like the case presented for Ni-EDTA complexes in Figure 22, the metal exchange reaction is favored at lower concentrations. Thus, even at the higher pH values in the sewage-contaminated zone, Zn-EDTA exchange with Fe would be increasingly favorable as time passed after injection, due to decreases in the concentrations of Zn-EDTA caused by dispersion and adsorption.

Modeling the Transport of Zn^{2+}

Reactive transport modeling of the results of the tracer test will require an appropriate model for adsorption reactions. Adsorption of the free metal ions displaced from metal-EDTA complexes resulted in their observed losses from the tracer cloud. Most of the mass of contaminant Zn is adsorbed to the sediments, and therefore it will be necessary to quantify Zn desorption in order to model transport of the metal-EDTA complexes in the Zn-contaminated region. Adsorption also caused retardation of Cr(VI) and the metal-EDTA complexes. Differences in chemical conditions between the pristine and sewage-contaminated zones affected the extent of adsorption, and thus, the retardation of these anionic solutes.

As shown in Figure 4, the leading edge of the Zn-contaminated region is approximately 155 m downgradient from the injection. When compared to the leading edge of nonreactive solutes in the sewage plume, the location of the leading edge of dissolved Zn suggests that Zn transport has been extensively retarded by adsorption onto the aquifer sediments (Kent et al., 2000). The upper and lower boundaries were quite sharp, as shown in Figure 2. The results of simulations conducted with a coupled flow and reactive transport model suggest that the sharpness of the upper boundary is maintained by the small vertical component to flow caused by areal recharge to the aquifer. The sharp lower boundary is caused by the increase in pH with depth, because the adsorption of Zn onto the sediments increases with increasing pH (Coston et al., 1995; Kent et al., 2000).

As a test of the applicability of the two-site surface complexation model (SCM) developed for Zn from batch studies described above, the SCM adsorption reactions were included in a modeling exercise to describe Zn transport after sewage effluent disposal. Simulations were conducted with HYDROGEOCHEM (Yeh and Tripathi, 1991), which allows the coupling of flow modeling with transport and chemical reactions. By including the SCM approach to describe adsorption, it was possible to test the influence of variable chemical conditions on the transport of Zn, which likely affects the observed spatial distribution of Zn contamination in the aquifer. The vertical gradient in pH within the Zn-contaminated region causes an increase in the extent to which Zn adsorbs on the Cape Cod sediments (Coston et al., 1995). Zn^{2+} introduced at the disposal beds is transported in the local flow field, and the extent of adsorption and retardation during transport is strongly influenced by the vertical gradient in pH. The model implemented coupled flow with advection, dispersion, and equilibrium adsorption in a 2-dimensional vertical cross section constructed along a flow line (Kent et al., 2000).

A steady-state flow model was constructed and the resulting flow field was used to set up the reactive transport simulations. The model included horizontal flow across the upgradient boundary and uniform areal recharge across the upper boundary and was calibrated using known head distributions, hydraulic conductivity measurements, and groundwater flow rates. Longitudinal and vertical transverse dispersivities were taken from Garabedian et al. (1991). The pH gradient was simulated by fixing the total dissolved CO_2 concentration of inflowing groundwater at 1 mM (millimoles per liter) and adjusting the ratio of H_2CO_3/HCO_3^- at each altitude to give the desired pH. The H_2CO_3/HCO_3^- ratio in the recharge water was chosen to give a pH of 5.5. A constant and uniform concentration of dissolved Zn^{2+} (8 μM) was input along the upgradient boundary to simulate the inflow of sewage-contaminated groundwater.

Results of a 60-year simulation computed using the 2-site surface complexation model are shown in Figure 26. Results of simulations conducted with the 1-site model were similar except that the leading edge of the Zn-contaminated region was much more diffuse. The reactive transport simulations capture the major features of the distribution of Zn-contamination in the aquifer as mapped in 1993 (Kent et al., submitted). Zn contamination migrated much farther at lower pH values near the top of the sewage plume than at the higher pH values observed deeper in the sewage effluent plume. In the downgradient region, the simulated Zn-contaminated region was relatively thin. The leading edge was located about 350 m downgradient from the effluent disposal beds (Figure 26), which corresponds to 112 m downgradient from the injection location in the field experiment presented in this report. This is somewhat less than was observed in the field (ca. 145 m downgradient from the injection location, Figure 4). However, unreactive constituents of the sewage plume migrated 7.9 km in the simulations (much farther than the observed 5.4 km), and thus the prediction of Zn retardation was very close to that observed in the field. The simulated Zn-concentration gradient across the leading edge was sharp in the two-site model, in agreement with the field data. Predicted Zn retardation was greater at the higher pH values present deeper in the sewage plume (Leading edge about 125 m downgradient of the disposal beds). This was in reasonable agreement with the few field observations made at these altitudes that suggest that Zn has been transported a distance on the order of 50-100 m (Rea et al., 1996; Kent et al., submitted). No fitting of the field data for Zn was done in these simulations; the predicted Zn distribution is a result of the two-site model derived from laboratory experimental data.

The results show that the two-site model (with a small number of parameters fit to laboratory data) can reasonably predict Zn transport for a range of chemical conditions. In comparison, a K_d modeling approach would require introducing a spatially variable range of K_d values because of the effects of pH and Zn concentration on K_d. Figure 27 shows the calculated dependency of K_d on pH and total Zn concentration for both the one-site and two-site surface complexation models derived from the laboratory experimental data. Note that only the two-site model has a significant dependence on the total Zn concentration.

The question of whether one-, two- or multiple-site adsorption models will be required in reactive transport modeling is important, because multiple site adsorption models increase the number of equations that must be solved. Transition metal cation adsorption on oxide minerals is characterized by constant pH isotherms that are nonlinear (e.g., Freundlich isotherms). Describing adsorption in these systems requires a surface complexation model with two or more sites, similar to that used for Zn on Cape Cod sediments (Davis et al., 1998). For example, Kohler et al. (1996) found that uranium transport under variable chemical conditions was poorly described by a one-site surface complexation model. However, a two-site model was able to describe and predict the key features of uranium transport over a range of chemical conditions. In contrast, one-site models can often predict anion adsorption onto pure hydrous metal oxides for a range of conditions (Dzombak and Morel, 1990). Even the effects of competition among adsorbing anions have been successfully predicted with one-site adsorption models for a range of chemical conditions (Zachara et al., 1987; Davis and Kent, 1990; Mesuere and Fish, 1992; Stollenwerk, 1995; Manning and Goldberg, 1996; Ali and Dzombak, 1996). One-site models may also be adequate for describing the adsorption of metal ions displaced from EDTA complexes (Equation 9), especially in the absence of significant metal contamination.

Concluding Remarks

Lessons learned from the modeling investigations that occur as a result of this study will have implications for parameter estimation that go far beyond the particular tracers studied here. Some important issues in reactive chemical parameter estimation are summarized in Table 9, based on the work of Rubin (1983, 1990). The upper panel summarizes how parameters may be estimated for chemical reactions for which local equilibrium can be assumed. For homogeneous reactions, chemical parameters consist of equilibrium constants taken from the literature, which are generally available. For classical heterogeneous reactions, i.e., dissolution equilibria, thermodynamic data for many crystalline solids are also available in the literature. However, the solubilities of poorly crystalline solids, impure solids, or solid solutions are generally not available and often will have to be determined experimentally with site-specific materials when relevant to a particular modeling application. Adsorption and other heterogeneous surface reactions will generally require experimental determination of parameters that are site-specific. Modeling of the Zn-contaminated region provides an example of how this might be accomplished.

Chemical reactions for which the local equilibrium assumption is not valid pose major challenges to predictive modeling of the fate and transport of reactive contaminants. For these systems, chemical reactions are classified into homogeneous reactions, heterogeneous reactions for which the overall rate is controlled by one or more chemical reaction steps, and heterogeneous reactions for which the overall rate is controlled by a physical process, such as diffusion or mixing across sediment layers. An example of the latter type of reaction is the transport of Cr(VI) in the suboxic zone, for which the rate of reduction was controlled by mixing of Cr(VI) into regions of the aquifer enriched in reductant (Friedly et al., 1995). Because the overall rate of reduction is controlled by a process linked to the sediment structure, rate parameters cannot be easily obtained from laboratory experiments since the sediment structure would be disturbed. In such cases, the appropriate rate parameters may need to be determined in field experiments. In this regard, it will be of interest to determine whether rate parameters derived from small-scale tracer tests can be applied in modeling the results of the large-scale test.

Evaluation of the critical issues in predictive transport modeling for reactive contaminants in groundwater awaits the testing of such models with well constrained experimental data. The design and execution of the reactive solute tracer test described here were conducted with this in mind. The chemical complexity and heterogeneity encountered within the spatial and temporal domain of the experiment were well characterized. Experimental data that describe the temporal and spatial distribution of the dissolved tracers were collected to the extent feasible, along with supplementary data, such as that describing metal speciation. Additional investigations will continue to determine which chemical reactions and processes were most important, in order to further enhance the usefulness of these experimental data in testing approaches to predictive modeling of the transport of reactive contaminants under variable chemical conditions.

References

Aggett, J. and Roberts, L.S. (1986) Insight into the mechanism of accumulation of arsenate and phosphate in Hydro Lake sediments by measuring the rate of dissolution with ethylenediaminetetraacetic acid (EDTA), Environ. Sci. Technol., 20, 183-186.

Ali, M.A. and Dzombak, D.A. (1996) Competitive sorption of simple organic acids and sulfate on goethite, Environ. Sci. Technol., 30(4), 1061-1071.

Anderson, L.D., Kent, D.B., and Davis, J.A. (1994) Batch experiments characterizing the reduction of Cr(VI) using suboxic material from a mildly reducing sand and gravel aquifer, Environ. Sci. Technol., 28(1), 178-185.

Barber, L.B., II (1990) Geochemical heterogeneity in a glacial outwash aquifer: Effect of particle size and mineralogy on sorption of nonionic organic solutes: Boulder, Colo., University of Colorado, Dept. of Geological Sciences, unpublished Ph.D. thesis, 238 pp.

Benjamin, M.M. and Leckie, J.O. (1981) Conceptual model for metal-ligand-surface interactions during adsorption, Environ. Sci. Technol., 15(9), 1050-1056.

Bhattacharyya, S.N. and Kunda, K.P. (1971) Spectrophotometric determination of EDTA, Talanta, 18, 446-449.

Borggaard, O.K. (1991) Effects of phosphate on iron oxide dissolution in EDTA and oxalate, Clays Clay Min., 39(3), 321-325.

Borggaard, O.K. (1976) Selective extraction of amorphous iron oxides by EDTA from a mixture of amorphous iron oxide, goethite and hematite, J. Soil Sci., 27, 478-486.

Borggaard, O.K. (1979) Selective extraction of amorphous iron oxides by EDTA from a Danish sandy loam, J. Soil Sci., 30, 727-734.

Bowers, A.R. and Huang, C.P. (1986) Adsorption characteristics of metal-EDTA complexes onto hydrous oxides, J. Colloid Interface Sci., 110(2), 575-590.

Bowers, A.R. and Huang, C.P. (1987) Role of Fe(III) in metal complex adsorption by hydrous solids, Water Res., 21(7), 757-764.

Brooks, S.C., Taylor, D.L., and Jardine, P.M. (1996) Reactive transport of EDTA-complexed cobalt in the presence of ferrihydrite, Geochim. Cosmochim. Acta, 60, 1899-1908.

Bryce, A.L., Kornicker, W.A. Elzerman, A.W., Clark, S.B. (1994) Nickel adsorption to hydrous ferric oxide in the presence of EDTA: Effects of component addition sequence, Environ. Sci. Technol., 28, 2353-2359.

Chang, H.C. and Matijevic, E. (1983) Interactions of metal hydrous oxides with chelating agents, J. Colloid Interface Sci., 92(2), 479-488.

Chao, T. T. and Zhou, L. (1983) Extraction techniques for selective dissolution of amorphous iron oxides from soils and sediments, Soil Sci. Soc. Amer. J., 47, 225-232.

Coston, J. A., Abrams, R. H., and Kent, D. B. (1998) Selected inorganic solutes, in Savoie, J. and LeBlanc, D. R., eds., Geochemical and hydrologic considerations in remediating phosphorus-contaminated ground water in a sewage plume near Ashumet Pond, Cape Cod Massachusetts, U.S. Geol. Survey Water-Resources Investigations Report 97-4269, p. 11-15.

Coston, J.A., Fuller, C.C., and Davis, J.A. (1995) Pb^{2+} and Zn^{2+} adsorption by a natural aluminum- and iron-bearing surface coating on an aquifer sand, Geochim. Cosmochim. Acta, 59(17), 3535-3547.

Davis, J. A., Hess, K. M., Coston, J. A., Kent, D. B., Joye, J. L., Brienen, P., Campo, K. W., (2000a) Multispecies reactive tracer test in a sand and gravel aquifer, Cape Cod, Massachusetts, Part I: Experimental design and transport of bromide and nickel-EDTA tracers, EPA/600/R-01/007a, 37 pp., U. S. Environmental Protection Agency.

Davis, J.A., Coston, J. A., Kent, D.B., and Fuller, C.C. (1998) Application of surface complexation concept to complex mineral assemblages, Environ. Sci. Technol., 32, 2820-2828.

Davis, J.A., Kent, D.B., Coston, J.A., and Hess, K.M. (1993a) Multi-species reactive solute transport experiment at the USGS research at Cape Cod, Massachusetts, 3. Minimization of the chemical reaction networks, EOS, Trans. Amer. Geophys. Union, 74, 280.

Davis, J. A., Kent, D. B., Coston, J. A., Hess, K. M., and Joye, J. L. (2000b) Multispecies reactive tracer test in an aquifer with spatially variable chemical conditions, Water Resour. Res., 36, 119-134.

Davis, J.A., Kent, D.B., Rea, B.A., Maest, A.S., and Garabedian, S.P. (1993b) Influence of redox environment and aqueous speciation on metal transport in groundwater: Preliminary results of tracer injection studies, *in* Allen, H.E., Perdue, E.M, and Brown, D.S., Eds., Metals in Groundwater, Chelsea, MI, Lewis Publishers, 223-273.

Davis, J.A. and Kent, D.B. (1990) Surface complexation modeling in aqueous geochemistry, Reviews in Mineralogy, 23, 177-260.

Dzombak, D.A., and Morel, F.M.M. (1990) Surface complexation modeling: Hydrous ferric oxide, New York, Wiley-Interscience, 393 pp.

Franson, M.A.H (1985) Standard methods for the examination of water and wastewater, 16th ed. American Public Health Association, Washington, D.C., p. 201-204.

Friedly, J.C., Davis, J.A., and Kent, D.B. (1995) Modeling hexavalent chromium reduction in ground water in field-scale transport and laboratory batch experiments, Water Resour. Res., 31(11), 2783-2794.

Fuller, C.C., Davis, J.A., Coston, J.A., and Dixon, E. (1996) Characterization of metal adsorption variability in a sand and gravel aquifer, Cape Cod, Massachusetts, U.S.A., J. Contam. Hydrol., 22, 165-187.

Garabedian, S. P., Leblanc, D. R., Gelhar, L. W., and Celia, M. A. (1991) Large-scale natural gradient tracer test in sand and gravel, Cape Cod, Massachusetts, 2. Analysis of spatial moments for a nonreactive tracer, Water Resour. Res., 27(5), 911-924.

Girvin, D.C., Gassman, P.L., and Bolton, H. (1993) Adsorption of aqueous cobalt ethylenediaminetetraacetate by $A1_2 0_3$, Soil Sci. Soc. Amer., 57, 47-57.

Gschwend, P.M., and M.D. Reynolds, (1987) Monodisperse ferrous phosphate colloids in an anoxic groundwater plume, J. Contam. Hydrol., 1 (3), 309-327.

Harvey, R.W. and Garabedian, S.P. (1991) Use of colloid filtration theory in modeling movement of bacteria through a contaminated sandy aquifer, Environ. Sci. Technol., 25(1), 178-185.

Hess, K. M, Davis, J. A., Coston, J. A., and Kent, D. B., (1999) Multispecies reactive transport under spatially variable chemical conditions: dispersion of bromide and nickel tracers, *in* U.S. Geological Survey Toxic Substances Hydrology Program — Proceedings of the Technical Meeting, Charleston, S. C., March 8-12, 1999, edited by D.W. Morganwalp, and H.T. Buxton, U.S. Geological Survey Water-Resources Investigations Report 99-4018C, pp 393-404.

Hess, K.M., Wolf, S.H., and Celia, M.A. (1992) Large-scale natural gradient tracer test in sand and gravel, Cape Cod, Massachusetts: 3. Hydraulic-conductivity variability and calculated macrodispersivities, Water Resour. Res., 28(8), 2011-2027.

Huang, C.P., Rhoads, E.A., Hao, O.J. (1988) Adsorption of Zn(II) onto hydrous aluminosilicates in the presence of EDTA, Water Res., 22(8), 1001-1009.

Jacobs, L.A., von Gunten, H.R., Keil, R., and Kuslys, M. (1988) Geochemical changes along a river-groundwater infiltration flow path: Glattfelden, Switzerland, Geochim. Cosmochim. Acta, 52, 2693-2706.

Kent, D.B., (1998) Effects of pumping rate and filtration on measured concentrations of inorganic solutes, J. Savoie, and D.R. LeBlanc, Eds.,U.S. Geological Survey Water-Resources Investigations Report 97-4269, pp. 11-15.

Kent, D. B., Abrams, R. H., Davis, J. A., Coston, J. A., and LeBlanc, D. R., (2000) Modeling the influence of variable pH on the transport of zinc in a contaminated aquifer using semi-empirical surface complexation models, Water Resour. Res., 36, 3411-3425.

Kent, D.B., Davis, J.A., Anderson, L.C.D., and Rea, B.A. (1995) Transport of chromium and selenium in a pristine sand and gravel aquifer: Role of adsorption processes, Water Resour. Res., 31(4), 1041-1050.

Kent, D.B., Davis, J.A., Anderson, L.C.D., Rea, B.A., and Waite, T.D. (1994) Transport of chromium and selenium in the suboxic zone of a shallow aquifer: Influence of redox and adsorption reactions, Water Resour. Res., 30(4), 1099-1114.

Kent, D.B., Davis, J.A., Rea, B.A., and Anderson, L.C.D. (1992) Ligand-enhanced transport of strongly adsorbing metal ions in the ground-water environment, in Kharaka, Y. and Maest, A.S., Eds., Water-Rock Interactions WRI-7, Rotterdam, A.A. Balkema, 1, 805-808.

Kent, D.B., Davis, J.A., Anderson, L.C.D., Rea, B.A., and Coston, J.A., Effect of adsorbed metal contaminants on the transport of Zn- and Ni-EDTA complexes in a sand and gravel aquifer, Environ. Sci. Technol., submitted.

Killey, R.W.D., McHugh, J.O., Champ, D.R., Cooper, E.L., and Young, J.L. (1984) Subsurface cobalt-60 migration from a low-level waste disposal site, Environ. Sci. Technol., 18, 148-157.

Kohler, M., Curtis, G.P., Kent, D.B., and Davis, J.A. (1996) Experimental investigation and modeling of uranium(VI) transport under variable chemical conditions, Water Resour. Res., 32(12), 3539-3551.

LeBlanc, D.R., Garabedian, S.P., Hess, K.M., Gelhar, L.W., Quadri, R.D., Stollenwerk, K.G., and Wood, W.W. (1991) Large-scale natural gradient tracer test in sand and gravel, Cape Cod, Massachusetts: 1. Experimental design and observed tracer movement, Water Resour. Res., 27(5), 895-910.

Lindsay and Walthall (1995) The solubility of aluminium in soils, in Sposito, G., Ed., The Environmental Chemistry of Aluminum, 2nd Edition, Boca Raton, FL, CRC Press, 333-361.

Liu, C.W. and Narasimhan, T.N. (1989) Redox-controlled multiple-species reactive chemical transport, 1, Model development, Water Resour. Res., 25, 869-882.

Manning, B.A. and Goldberg, S. (1996) Modeling competitive adsorption of arsenate with phosphate and moybdate on oxide minerals, Soil Sci. Soc. Amer., 60, 121-131.

Martell, A.E. and Smith, R.M. (1989) Critical Stability Constants, Vol. 6, Second Supplement, New York, Plenum, 604 pp.

McBride, M. B., Richards, B. K., Steenhuis, T., Russo, H. J., and Sauve, S. (1997) Mobility and solubility of toxic metals and nutrients in soil fifteen years after sludge application, Soil Sci., 162, 487-500.

McCarthy, J. F., Czerwinski, K. R., Sanford, W. E., Jardine, P. M., and Marsh, J. D. (1998) Mobilization of transuranic radionuclides from disposal trenches by natural organic matter, J. Contam. Hydrol., 30, 49-77.

Mesuere, K. and Fish, W. (1992) Chromate and oxalate adsorption on goethite (a-FeOOH), Environ. Sci. Technol., 26, 2365-2370.

Morel, F.M.M. and Hering, J.G. (1993) Principles and applications of aquatic chemistry, New York, John Wiley, 588 pp.

Nowack, B., Lutzenkirchen, J., Behra, P., and Sigg, L. (1996) Modeling the adsorption of metal-EDTA complexes onto oxides, Environ. Sci. Technol., 30, 2397-2405.

Nowack, B. and Sigg, L. (1996) Adsorption of EDTA and metal-EDTA complexes on goethite, J. Colloid Interface Sci., 177, 106-121.

Nowack, B. and Sigg, L. (1997) Dissolution of Fe(III) (hydr)oxides by metal-EDTA complexes, Geochim. Cosmochim. Acta, 61, 951-963.

Oldale, R. N. and Barlow, R.A. (1986) Geologic map of Cape Cod and the Islands, Massachusetts, U.S. Geological Survey, Miscellaneous Investigations Series, Map I-1763, 1 plate.

Papelis, C., Hayes, K.F., and Leckie, J.O. (1988) HYDRAQL: A program for the computation of chemical equilibrium composition of aqueous batch systems including surface-complexation modeling of ion adsorption at the oxide/ solution interface, Dept. of Civil Engineering, Stanford University, Technical Report, 306, 130 pp.

Rea, B.A., Kent, D.B., Anderson, L.C.D., Davis, J.A., and LeBlanc, D.R. (1996) The transport of inorganic contaminants in a sewage plume in the Cape Cod aquifer, Massachusetts, in Morganwalp, D.W. and Aronson, D.A., Eds., U.S. Geological Survey Toxic Substances Hydrology Program—Proceedings of the technical meeting, Colorado Springs, Colorado, September 20-24, 1993; U.S. Geological Survey Water-Resources Investigations Report, 94-4015, 191-198.

Rea, B.A., Davis, J.A., and Waychunas, G.A. (1994) Studies of the reactivity of the ferrihydrite surface by iron isotopic exchange and Mossbauer spectroscopy, Clays Clay Min.,42, 23-34.

Rea, B.A., Kent, D.B., LeBlanc, D.R., and Davis, J.A. (1991) Mobility of zinc in a sewage-contaminated aquifer, Cape Cod, Massachusetts, *in* Mallard, G.E. and Aronson, D.A., Eds., U.S.Geological Survey Toxic Substances Hydrology Program—Proceedings of the technical meeting, Monterey, California, March 11-15, 1991, U.S. Geological Survey Water-Resources Investigations Report, 91-4034, 88-95.

Roberts, P.V., Goltz, M.N., and Mackay, D.M. (1986) A natural gradient experiment on solute transport in a sand aquifer, 3. Retardation estimates on mass balances for organic solutes, Water Resour. Res., 22(13), 2047-2058.

Roy, S.B., and D.A. Dzombak, Colloid release and transport processes in natural and model porous media, Colloids Surf., 107, 245-262, 1996.

Roy, S.B., and D.A. Dzombak, Chemical factors influencing colloid-facilitated transport of contaminants in porous media, Environ. Sci. Technol., 31, 656-664, 1997.

Rubin, J. (1983) Transport of reacting solutes in porous media: Relation between mathematical nature of problem formulation and chemical nature of reactions, Water Resour. Res., 19,1231-1252.

Rubin, J. (1990) Solute transport with multisegment, equilibrium-controlled reactions: A feed forward simulation method, Water Resour. Res., 26(9), 2029-2055.

Smith, R.M. and Martell, A.E. (1989) Critical Stability Constants, 6, Second Supplement, New York, Plenum, 643 pp.

Stollenwerk, K.G. (1995) Modeling the effects of variable groundwater chemistry on adsorption of molybdate, Water Resour. Res., 31(2), 347-357.

von Gunten, H.R., Karametaxas, G., Krahenbuhl, U., Kuslys, M., Giovanoli, R., Hoehn, E., and Keil, R. (1991) Seasonal biogeochemical cycles in riverborne groundwater, Geochim. Cosmochim. Acta, 55(12), 3597-3609.

White, A.F. and Peterson, M.L. (1996) Reduction of aqueous transition metal species on the surfaces of Fe(II)-containing oxides, Geochim. Cosmochim. Acta, 60(20), 3799-3814.

Yeh, G.T. and Tripathi, V.S. (1991) A model for simulating transport of reactive multispecies components: Model development and demonstration, Water Resour. Res., 27(12), 3075-3094.

Yu, J. and Klarup, D. (1993) Extraction kinetics of copper, zinc, iron, and manganese from contaminated sediment using disodium ethylenediaminetetraacetate, Amer. Chem. Soc., 205th National meeting, Denver, CO, 33(1), 69-72.

Zachara, J.M., Gassman, P.L., Smith, S.C., and Taylor, D. (1995a) Oxidation and adsorption of Co(II)-EDTA complexes in subsurface materials with iron and manganese oxide grain coatings, Geochim. Cosmochim. Acta, 59(21), 4449-4464.

Zachara, J.M., Smith, S.C., and Kuzel, L.S. (1995b) Adsorption and dissociation of Co-EDTA complexes in iron oxide-containing subsurface sands, Geochim. Cosmochim. Acta, 59(23), 4825-4844.

Zachara, J.M., Girvin, D.C., Schmidt, R.L., and Resch, C.T. (1987) Chromate adsorption on amorphous iron oxyhydroxide in the presence of major groundwater ions, Environ. Sci. Technol., 21, 589-594.

Zapico, M.M., Vales, S. and Cherry, J.A. (1987) A wireline piston core barrel for sampling cohesionless sand and gravel below the water table, Ground Water Monit. Rev., 7(3), 74-82.

Tables

Table 1. Data for the Breakthrough MLS, BT1 (37 m downgradient) [Areas under the Breakthrough Curves for Br and the Ratio of Areas for Reactive Tracers to Br Areas]

	Area, days	*Area(i)/ Area(Br)*							
Altitude, m	***Br***	***EDTA***	***Cr***	***Cu***	***Ni***	***Zn-total***	***'free' Zn***	***Al***	***FeT***
Pristine zone									
13.51	n/s	n/s	0	0	0	0	n/s	0	0
13.21	n/s	0	[0.40]	0	0	0	n/s	0	[0.15]
12.90	0.44	1.01	2.84	0.02	0.75	0.26	0	0	1.31
12.60	1.24	0.79	1.13	0.56	0.66	0.49	n/s	0	0.47
Zn-contaminated region									
12.14	2.65	0.59	0.63	0.70	0.78	1.17	0.24	0.01	0.22
11.68	2.29	0.90	1.06	0.83	1.04	2.19	n/s	0	0.22
11.23	3.32	0.84	0.80	0.77	0.97	2.17	0.52	0	0.18
10.77	4.30	0.65	0.53	0.49	0.75	2.42	n/s	0	0.13
10.30	3.23	0.84	0.55	0.63	0.97	3.30	0.58	0	0.13
Sewage-contaminated zone									
9.85	3.75	1.04	0.40	0.75	1.09	2.52	n/s	0	0.16
9.39	5.12	0.94	0.06	0.98	1.07	0.85	n/s	0	0.19
8.93	1.24	0.86	0	0.77	0.86	0.23	n/s	0	0.20
8.47	0.57	0.58	0	0.15	0.31	0	n/s	0	0.13
8.02	2.27	0.70	0	0.55	0.74	0.25	n/s	0.01	0.24
7.56	0.16	1.20	0	0.84	0.98	0.15	n/s	0	0.26

n/s = samples not collected

[] indicates the area under the breakthrough curve of a constituent at an elevation where no Br was measurable.

Table 2. Data for the Breakthrough MLS, BT2 (52 m downgradient) [Areas under the Breakthrough Curves for Br and the Ratio of Areas for Reactive Tracers to Br Areas (Al Was Not Detected at this MLS)]

	Area, days	*Area(i)/ Area(Br)*						
Altitude, m	***Br***	***EDTA***	***Cr***	***Cu***	***Ni***	***Zn-total***	***'free' Zn***	***FeT***
Pristine zone								
13.65	n/s	n/s	0	0	0	0	n/s	0
13.14	0.03	0	0	0	0	1.68	n/s	2.02
12.63	0.89	0.99	0.79	0.14	0.46	0.64	0.06	0.72
Zn-contaminated region								
12.13	2.85	0.65	0.75	0.57	0.72	1.25	n/s	0.25
11.62	2.90	0.84	0.72	0.62	1.12	2.02	0.97	0.30
11.11	3.48	0.72	0.57	0.48	0.87	2.32	n/s	0.22
10.60	4.20	0.92	0.69	0.67	1.12	3.10	1.52	0.20
10.10	4.29	0.98	0.39	0.57	1.17	2.90	n/s	0.21
Sewage-contaminated zone								
9.59	3.54	0.98	0.12	0.75	1.06	1.91	0.84	0.21
9.08	2.06	0.88	0	0.70	0.88	0.11	n/s	0.25
8.58	0.89	1.54	0	1.30	1.59	0.13	n/s	0.43
8.07	0.53	0.97	0	0.69	0.93	0.11	n/s	0.35
7.56	0.06	1.03	0	0.19	0.32	0.32	n/s	0.17
7.05	n/s	0	0	0	0	0	n/s	0
6.54	n/s	0	0	0	0	0	n/s	0

n/s = samples not collected

Table 3. Data for the Breakthrough MLS, BT1 (37 m downgradient) [Estimated Retardation Factors]

	Avg. $<t_i>$ days	*Average R_f, $<t_i>/<t_{Br}>$*							
Altitude, m	***Br***	***EDTA***	***Cr***	***Cu***	***Ni***	***Zn-total***	***'free' Zn***	***Al***	***Fe***
Pristine zone									
13.51	n/s	n/s	0	0	0	0	n/s	0	0
13.21	n/s	0	[159]	0	0	0	n/s	0	[86.9]
12.90	61.2	1.34	2.32	2.02	2.07	2.73	0	0	1.33
12.60	56.7	1.32	1.70	1.53	1.38	1.65	n/s	0	1.28
Zn-contaminated region									
12.14	67.4	1.16	1.28	1.23	1.17	1.24	1.14	1.12	1.10
11.68	82.1	1.22	1.28	1.26	1.21	1.24	n/s	0	1.11
11.23	77.7	1.16	1.23	1.19	1.15	1.20	1.29	0	1.07
10.77	67.9	1.10	1.15	1.12	1.10	1.18	n/s	0	1.05
10.30	71.0	1.04	1.07	1.05	1.04	1.13	1.14	0	1.02
Sewage-contaminated zone									
9.85	85.5	1.07	1.10	1.09	1.06	1.08	n/s	0	1.04
9.39	94.2	1.06	1.09	1.07	1.05	1.05	n/s	0	1.04
8.93	97.7	0.96	0	0.96	0.94	0.96	n/s	0	0.93
8.47	93.1	1.01	0	1.08	1.09	0	n/s	0	1.03
8.02	90.0	1.04	0	1.04	1.03	1.04	n/s	1.02	1.01
7.56	79.1	1.05	0	1.03	1.03	1.02	n/s	0	1.01

n/s = samples not collected

[ ]indicates the area under the breakthrough curve of a constituent at an elevation where no Br was measurable.

Table 4. Data for the Breakthrough MLS, BT2 (52 m downgradient) [Estimated Retardation Factors (Al was not detected at this MLS)]

Altitude, m	*Avg. $<t_i>$ days*	*Average R_f, $<t_i>/<t_{Br}>$*						
	Br	***EDTA***	***Cr***	***Cu***	***Ni***	***Zn-total***	***'free' Zn***	***Fe***
Pristine zone								
13.65	n/s	n/s	0	0	0	0	n/s	0
13.14	82.7	0	0	0	0	2.15	n/s	1.34
12.63	78.3	1.14	1.87	1.81	1.67	1.63	1.08	1.17
Zn-contaminated region								
12.13	96.9	1.30	1.36	1.34	1.27	1.31	n/s	1.14
11.62	111	1.14	1.18	1.16	1.13	1.15	1.19	1.06
11.11	98.2	1.14	1.17	1.14	1.11	1.21	n/s	1.06
10.60	95.5	1.07	1.11	1.10	1.07	1.18	1.35	1.04
10.10	114	1.08	1.14	1.10	1.07	1.09	n/s	1.03
Sewage-contaminated zone								
9.59	125	1.10	1.21	1.12	1.09	1.06	1.03	1.05
9.08	134	1.07	0	1.08	1.06	1.09	n/s	1.03
8.58	126	1.13	0	1.16	1.13	1.17	n/s	1.07
8.07	110	1.07	0	1.06	1.03	1.17	n/s	1.01
7.56	99.1	1.04	0	1.05	1.04	1.55	n/s	1.02
7.05	n/s	0	0	0	0	0	n/s	0
6.54	n/s	0	0	0	0	0	n/s	0

n/s = samples not collected

Table 5. Dissolution of Al, Fe, and Zn from Aquifer Composite Sediments by Hydroxylamine-HCl and EDTA

	Pristine		***Sewage-contaminated***		***Zn-contaminated***		
Surface Area, m^2/g	0.36		0.33		0.24		
Conditions	***Al***	***Fe***	***Al***	***Fe***	***Al***	***Fe***	***Zn***
Hydroxylamine-HCl extraction, μmoles/m^2	10.3	1.61	6.55	1.70	14.1	3.08	0.46
Apparent EDTA dissolution rates	***pH 5.4***		***pH 6.5***		***pH 6.5***		
Fast reaction, μmoles/m^2 – hour	0.040	0.0019	0.018	0.007	0.014	0.017	0.0003
Intercept, μmoles/m^2	0.32	0.16	0.020	0.076	0.066	0.062	0.008
R^2	0.83	0.96	0.99	0.84	0.85	0.96	0.94
Time range, hours	*0.5-4*	*0.5-216*	*0.5-8*	*0.5-48*	*0.5-24*	*0.5-24*	*0.5-48*
Slow reaction, μmoles/m^2 - hour	None	0.0005	0.0014	0.0006	None	0.001	None
Intercept, μmoles/m^2		0.42	0.16	0.33		0.39	
R^2		0.95	0.98	0.99		0.83	
Time range, hours		*216-336*	*8-48*	*48-336*		*24-336*	

none = metal-EDTA complex is undergoing resorption and exchange back reaction.

Table 6. Stability Constants of Metal Exchange Reactions with Aqueous Metal Ions

Me	***Log K***
Cu^{2+}	9.5
Ni^{2+}	9.9
Pb^{2+}	10.3
Zn^{2+}	11.8

Table 7. Stability Constants for Metal Ion Adsorption on Ferrihydrite

Me	*Log K*
Ni^{2+}	0.4
Zn^{2+}	1.0
Cu^{2+}	2.9
Pb^{2+}	4.7

Table 8. Stability Constants of Metal Exchange Reactions with Adsorbed Metal Ions

Me	*Log K*
Ni^{2+}	10.3
Cu^{2+}	12.4
Zn^{2+}	12.8
Pb^{2+}	15.0

Table 9. Issues Facing Estimation of Chemical Parameters in Reactive Transport Models

Level	Class	Parameter Estimation
"Sufficiently Fast" and Reversible	Homogeneous	Literature
	Heterogeneous Classical	Literature and using established laboratory experimental procedures (poorly characterized participants)
	Heterogeneous Surface	Site-specific parameters, require laboratory experiments
"Insufficiently Fast"	Homogeneous	Probably can be determined in laboratory experiments
	Heterogeneous Chemical-control	Might be determined in laboratory experiments; conceptual hurdles.
	Heterogeneous Physical-control	Process controlling rate linked to sediment structure. Field experiments required.

Figures

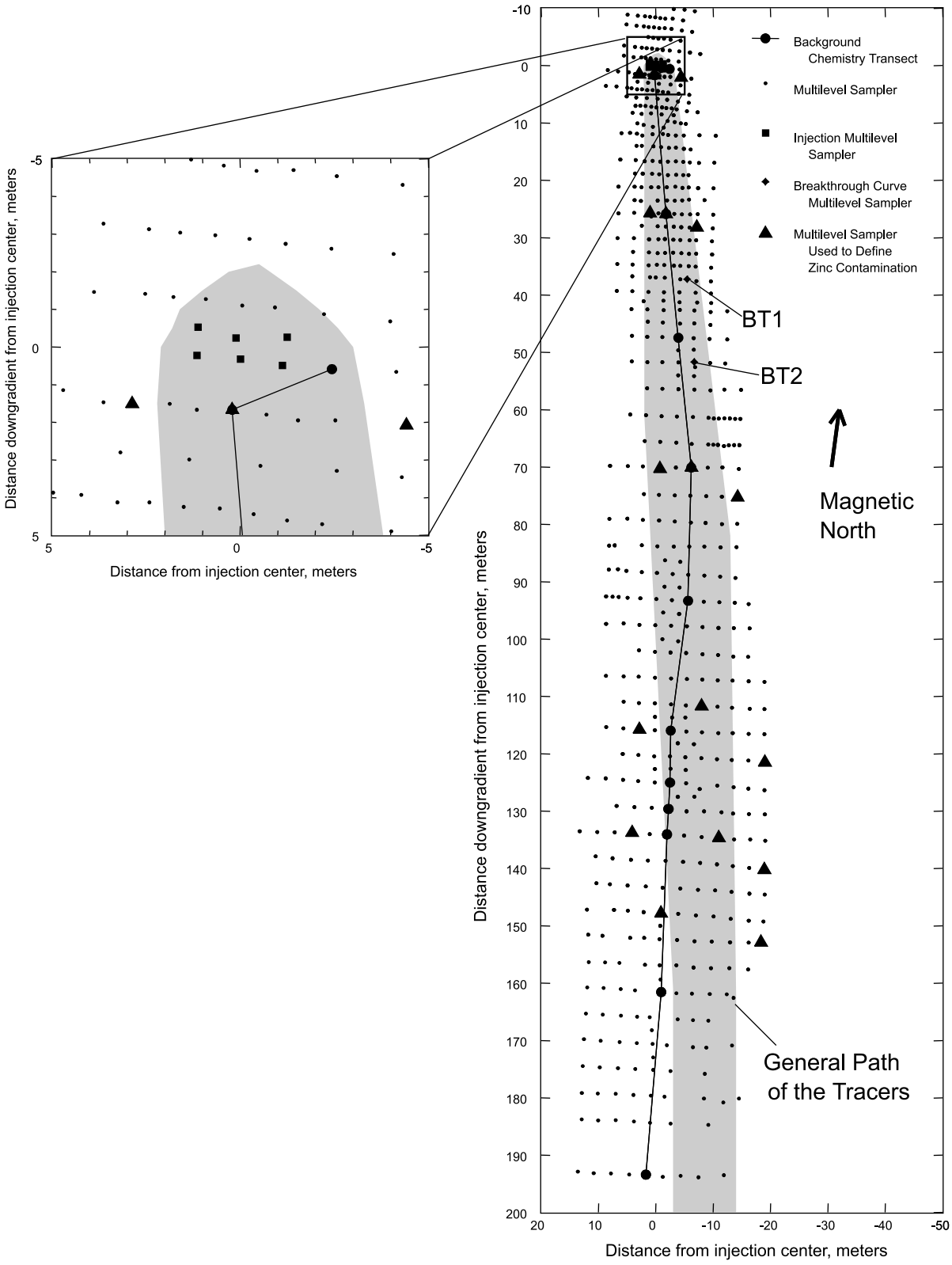

Figure 1. Location of tracer-test site in western Cape Cod, Massachusetts, the general path of tracers, the multilevel samplers (MLS) available for sampling during the tracer test, the six injection MLS, the two breakthrough curve MLS, and the MLS used to construct background chemistry transects and to define the extent of zinc contamination.

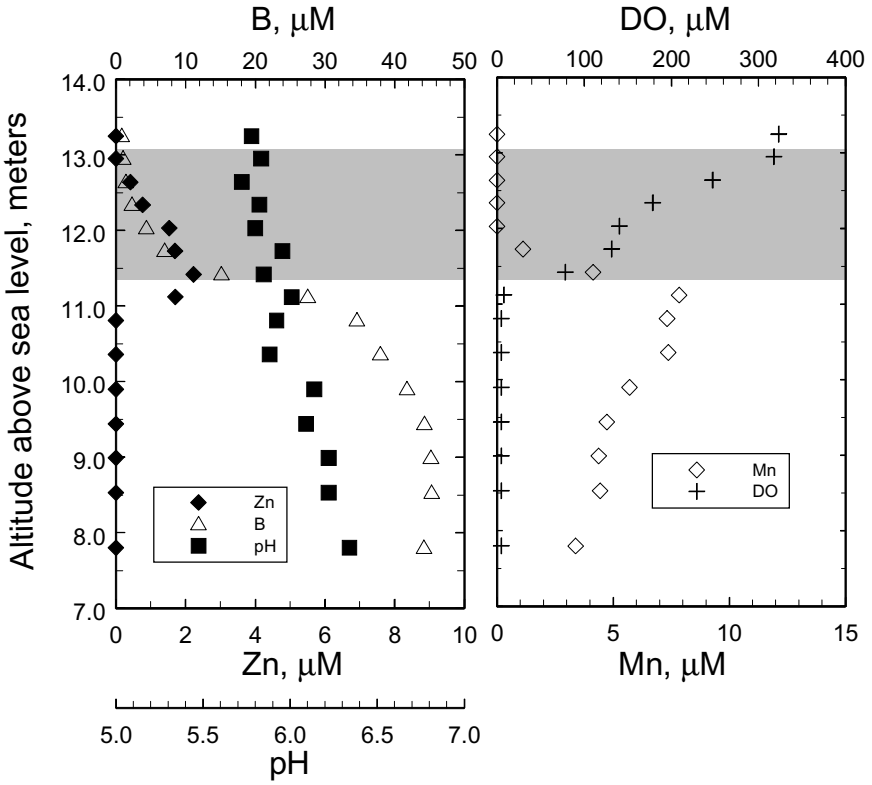

Figure 2. Vertical profiles of B (boron), Zn (zinc), pH, DO (dissolved oxygen), and Mn (manganese) 1.7 m downgradient from the center of the injection taken just prior to injection at MLS 2414A (shown in inset of Fig. 1 as filled triangle closest to the array of injection MLS). The shaded area shows the location of the Zn-contaminated region for this MLS.

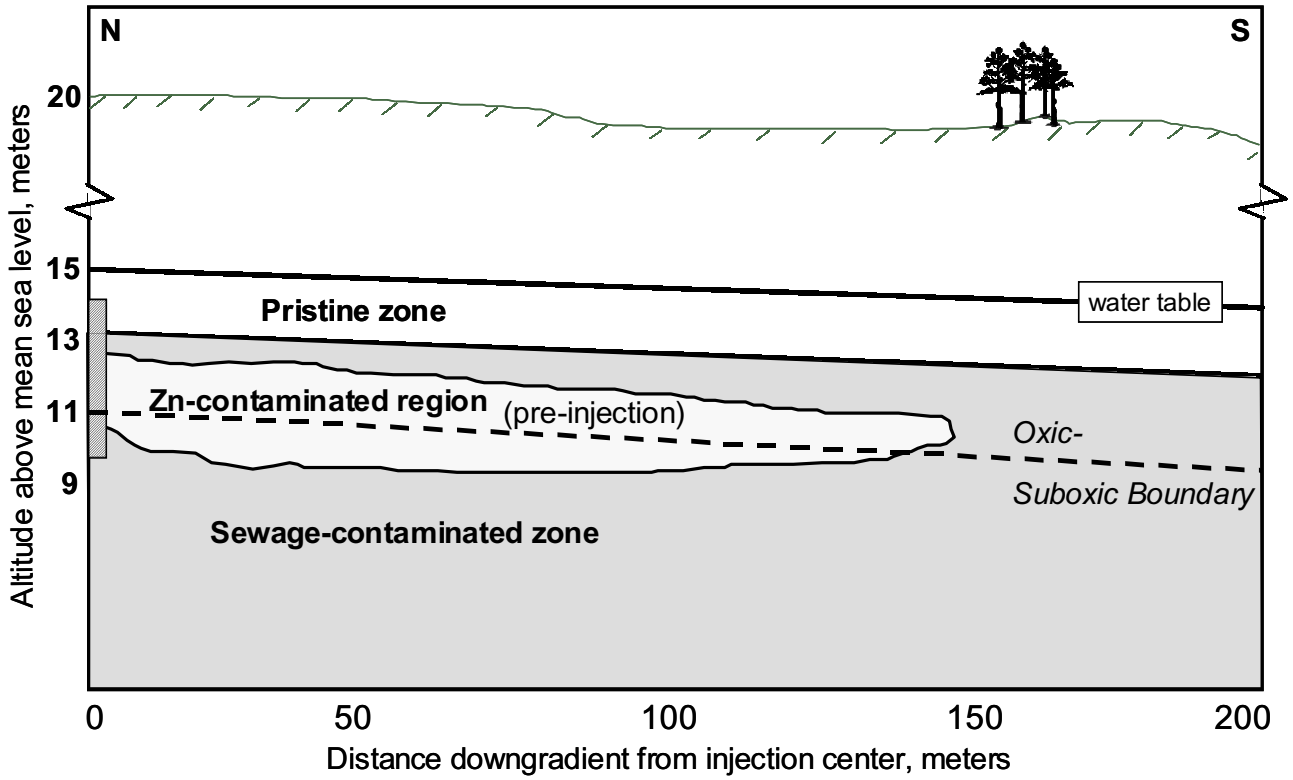

Figure 3. Schematic showing the relative locations of geochemical zones referred to in this report.

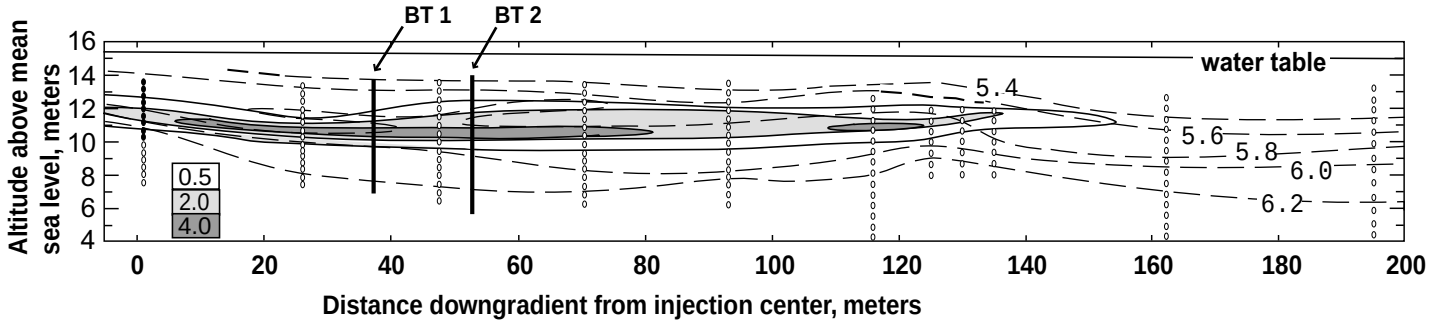

Figure 4. Longitudinal cross section showing the concentration of dissolved Zn (μM) and pH in the aquifer prior to the field experiment. The area shown is downgradient from the injection location. Location of the transect is shown in Figure 1. The small circles indicate the locations where groundwater was collected. The filled small circles indicate the ports in which Br and reactive tracers were detected in samples taken just after the injection. The vertical extent covered by the two breakthrough MLS (BT1 and BT2) is indicated by the solid bars.

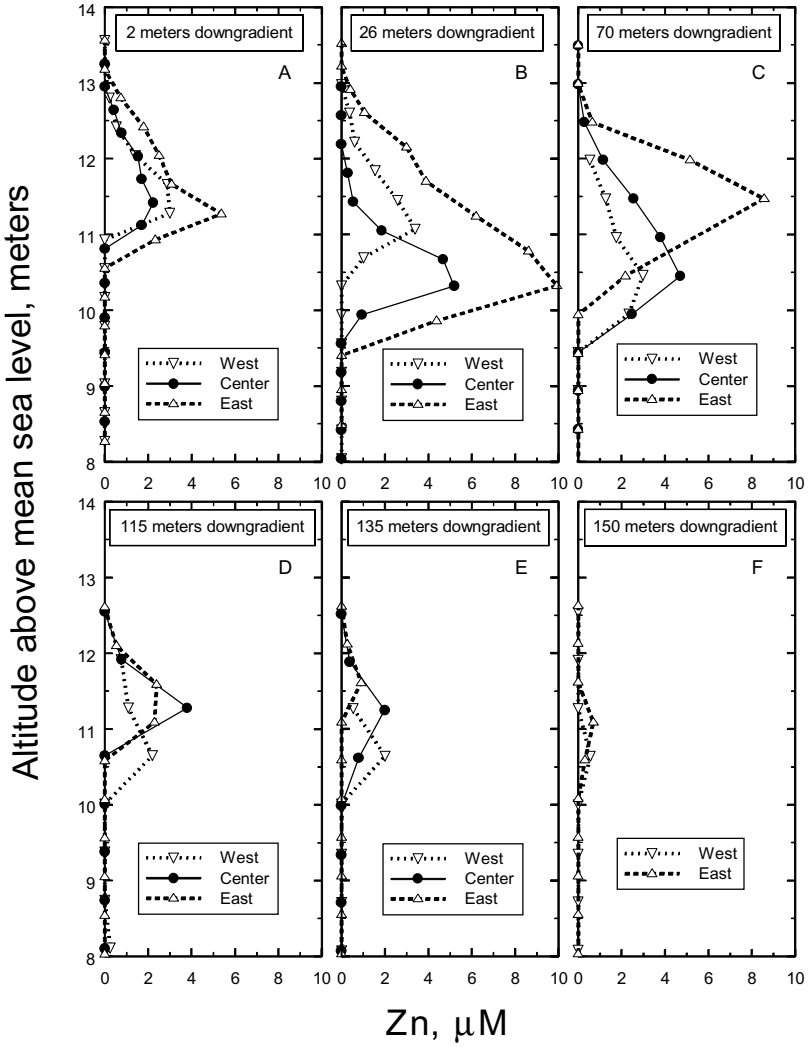

Figure 5. Vertical profiles showing longitudinal and lateral heterogeneity in the distribution of background dissolved Zn in the aquifer. Panels A through F show sets of dissolved Zn profiles taken approximately 2, 26, 70, 115, 135, and 150 meters downgradient, respectively. Each panel shows vertical profiles taken west of the region traversed by the tracer cloud, near the center of the region traversed by the tracer cloud, and east of the region traversed by the tracer cloud. Locations of MLS used to construct these profiles are shown as filled triangles in Figure 1.

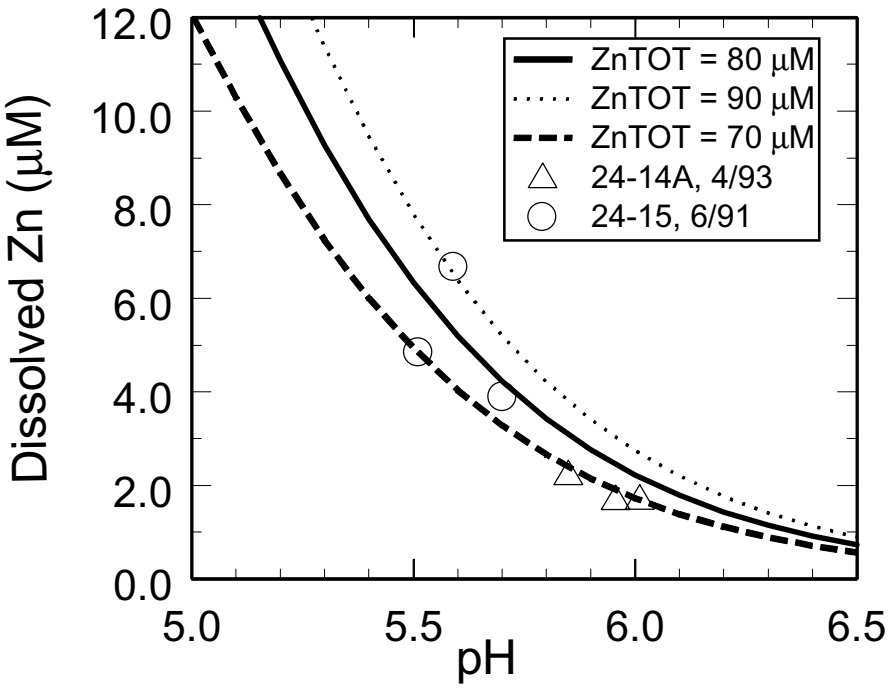

Figure 6. Dissolved Zn as a function of pH. Curves show Zn concentrations versus pH for three values of total Zn (adsorbed plus dissolved), computed from the surface complexation model fitted to batch adsorption data (Davis et al., 1998). Also shown are data from MLS 2415, sampled in June of 1991, and 2414A, sampled before the injection (Fig. 2). The two MLS are adjacent to one another and the three data points come from the same altitude range (11.3 to 12.0 m to sea level). Location of MLS 2414A is shown in inset of Figure 1 (filled triangle closest to the array of injection MLS).

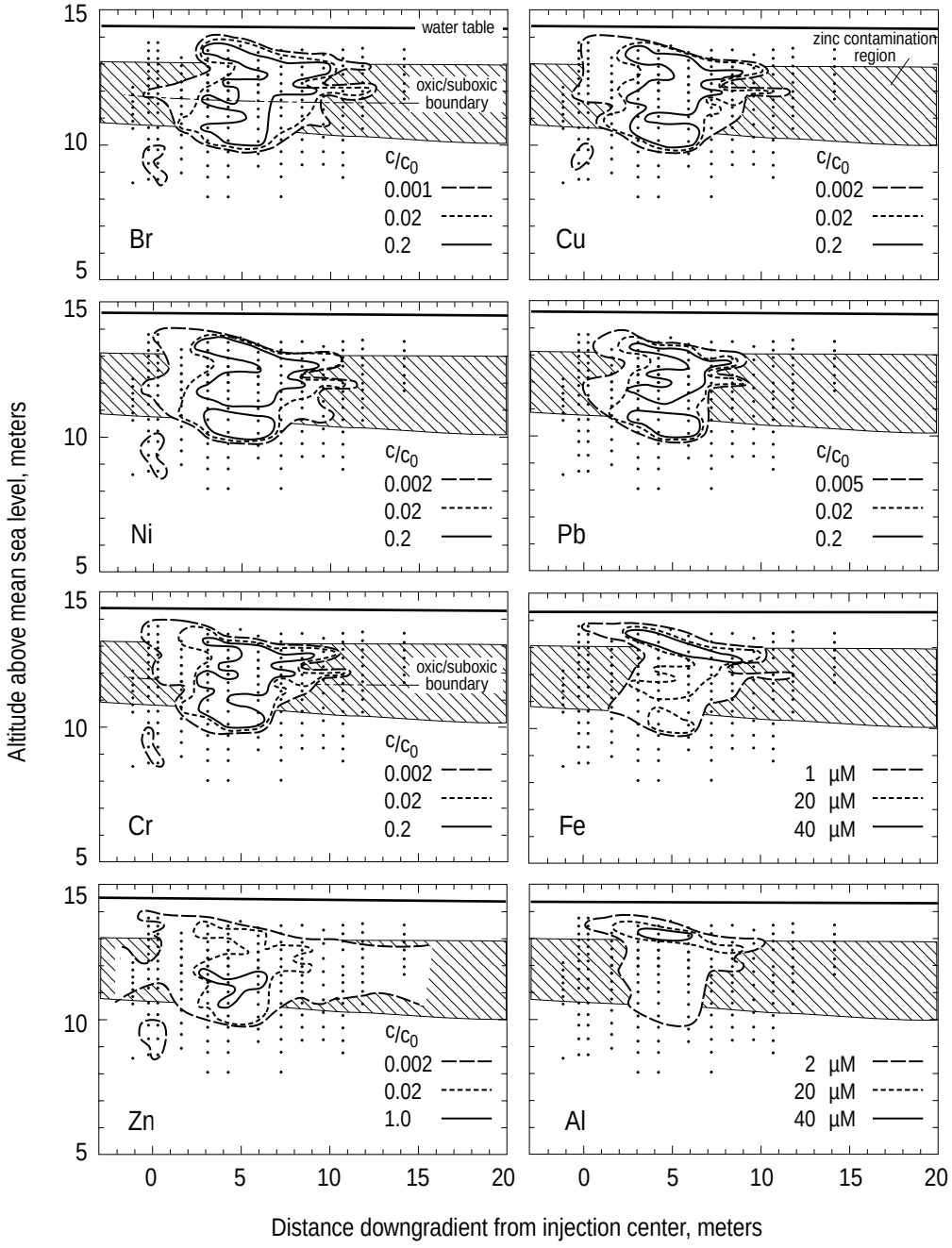

Figure 7. Longitudinal cross sections showing the normalized concentrations of the tracers Br, Ni, Cr, Zn, Cu, and Pb and the dissolved concentrations of Fe and Al, 13 days after the injection. The Zn-contaminated region is also shown. Dissolved oxygen was 3 µM or less prior to the injection at altitudes below the oxic/suboxic boundary shown on the figure. The boundary is located within the Zn-contaminated region.

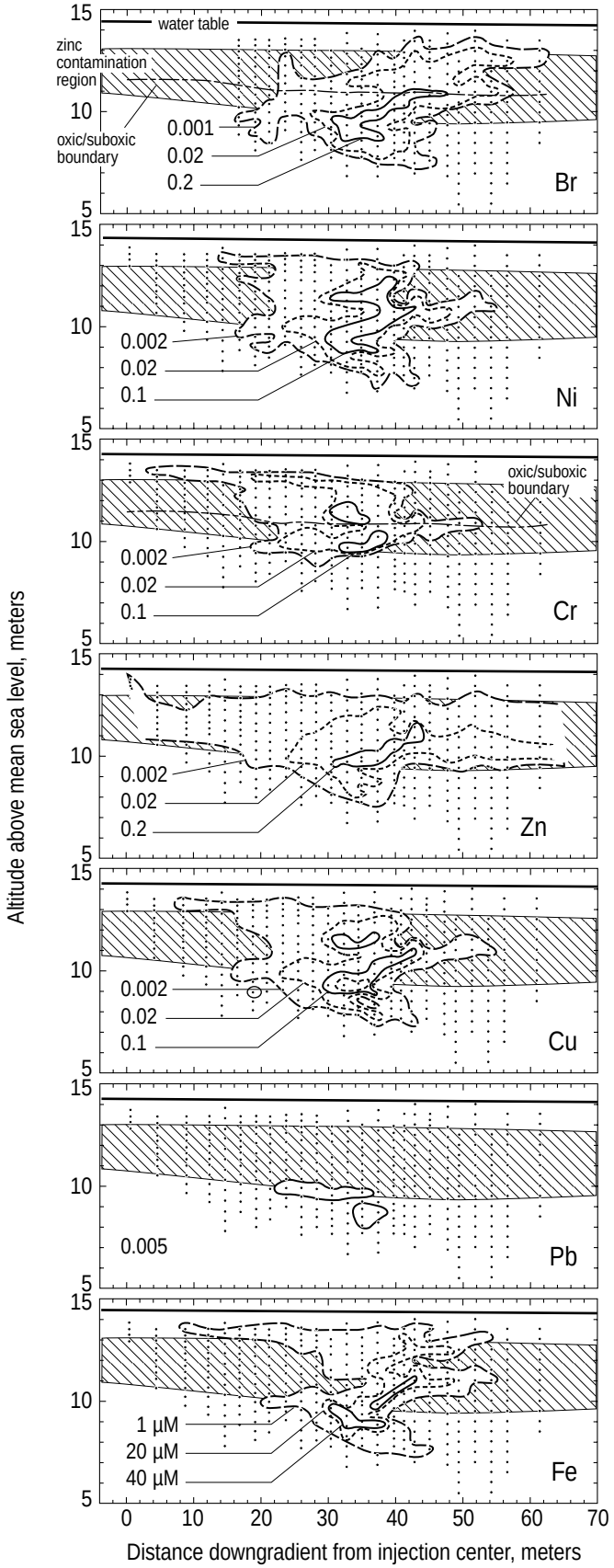

Figure 8. Longitudinal cross sections showing the normalized concentrations of the tracers Br, Ni, Cr, Zn, Cu, and Pb and the dissolved concentration of Fe 83 days after the injection. The Zn-contaminated region and oxic/suboxic are same as in Figure 7.

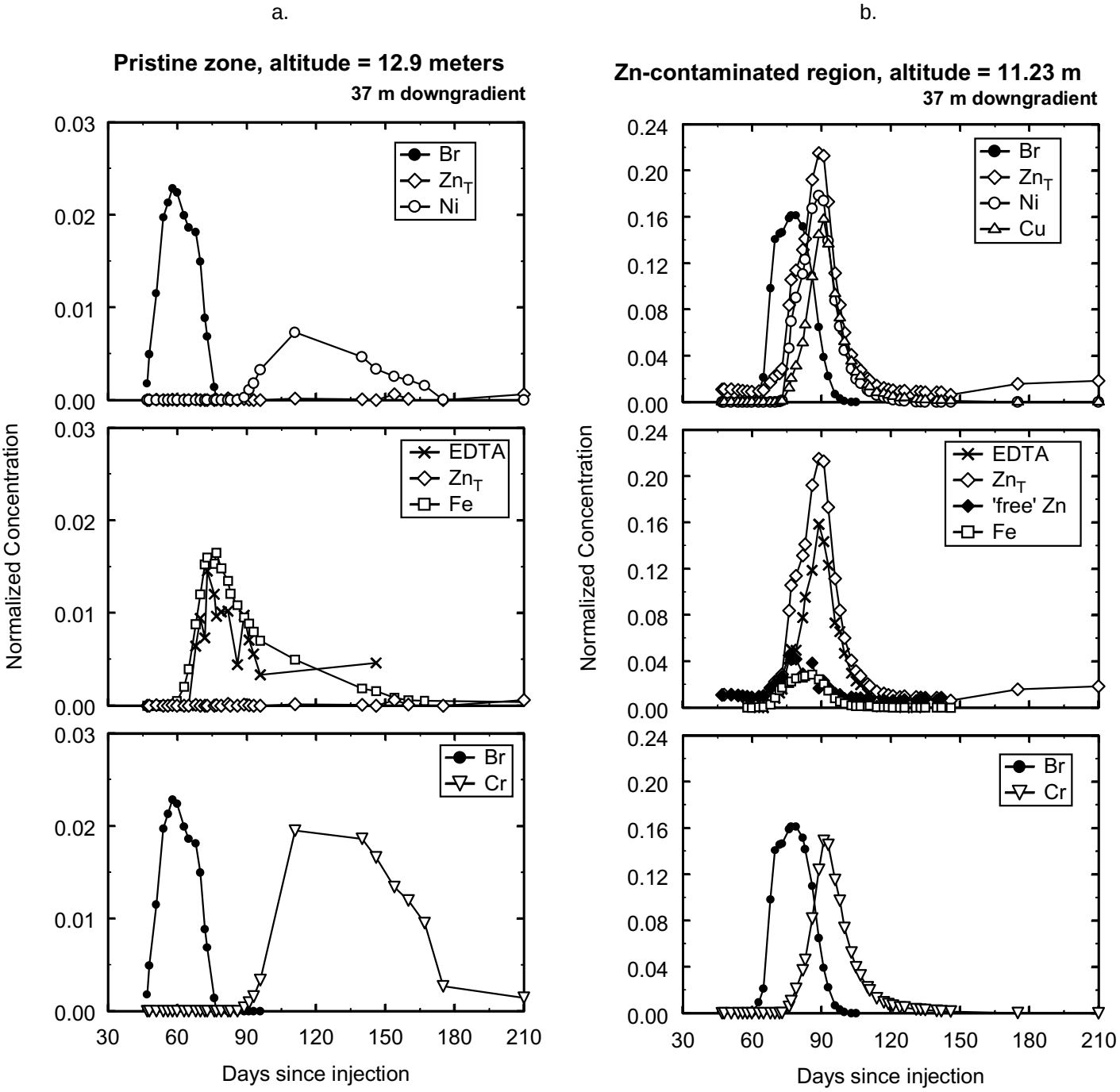

Figure 9. Breakthrough curves for BT1, 37 m downgradient of the injection site. Concentrations are normalized to the injectate concentrations for each element, except Fe, which is normalized to the concentration of injected EDTA: a.) pristine zone; b.) upper Zn-contaminated region; c.) lower Zn-contaminated region; d.) upper sewage-contaminated zone, below Zn contamination; e.) lower sewage-contaminated zone.

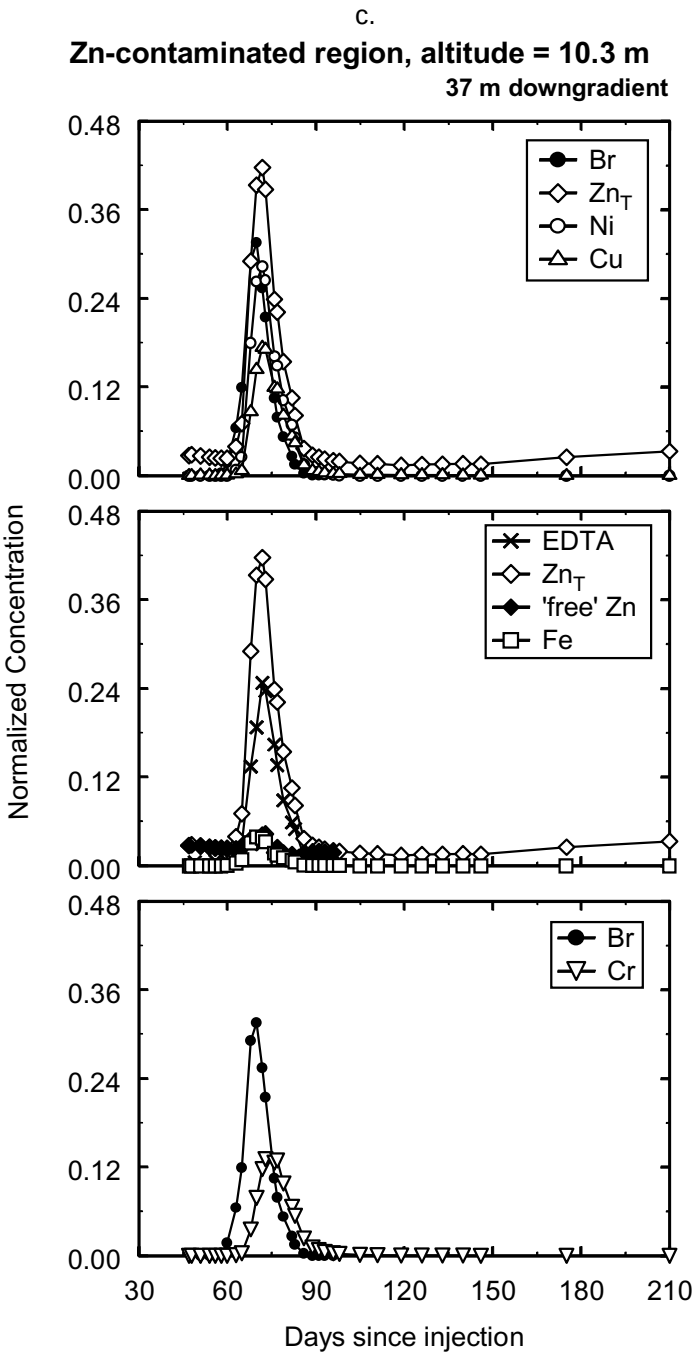

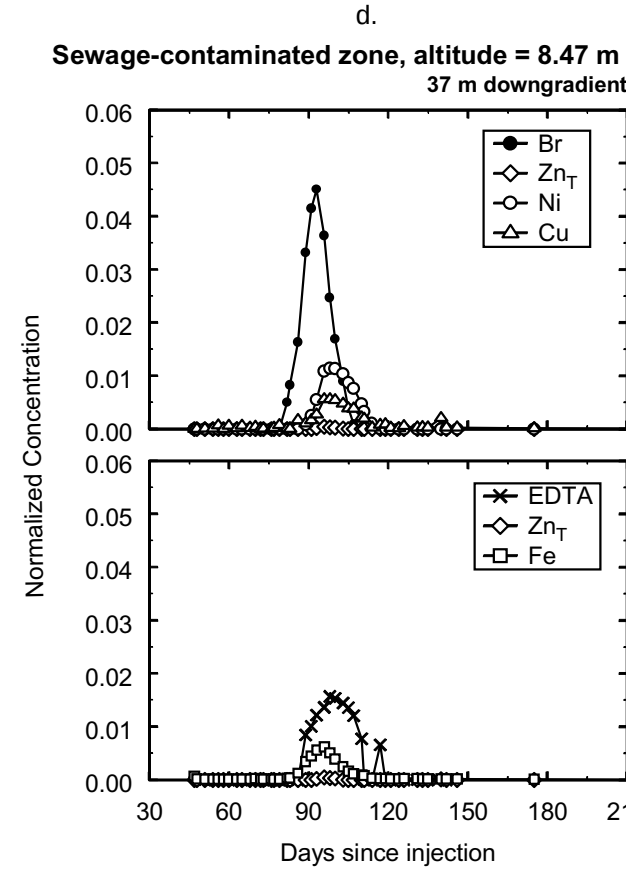

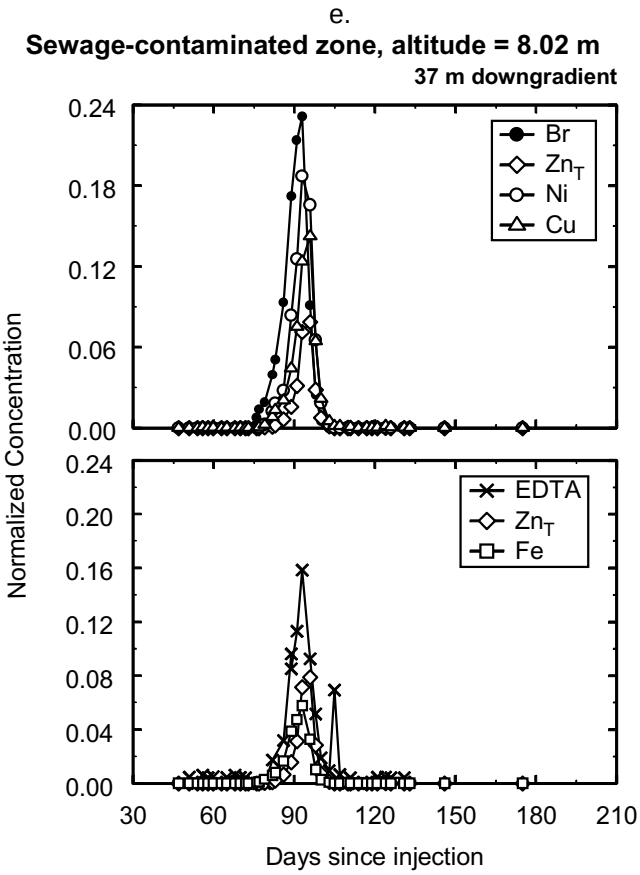

Figure 9. Continued.

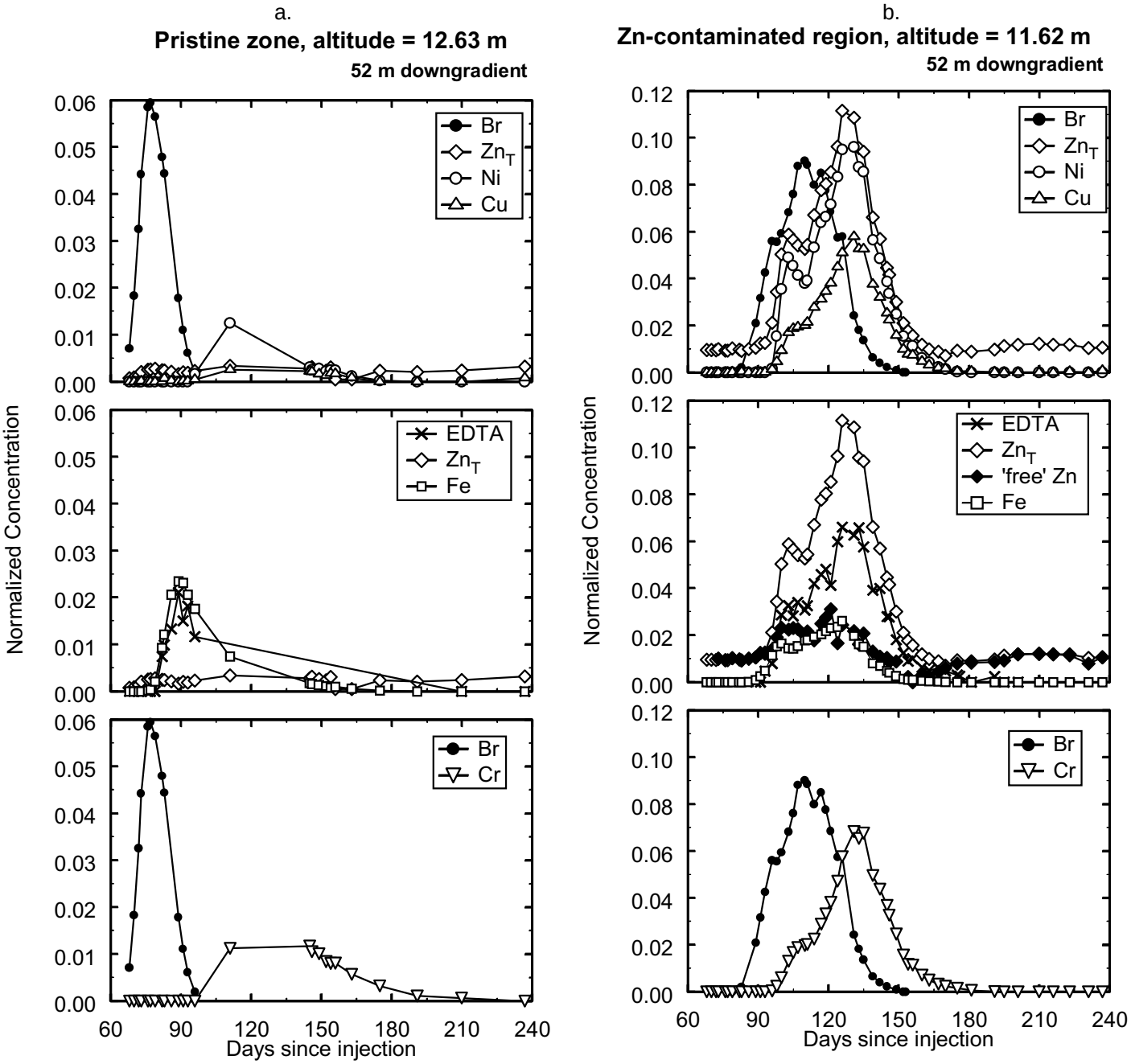

Figure 10. Breakthrough curves for BT2, 52 m downgradient of the injection site. a.) pristine zone; b.) upper Zn-contaminated region; c.) lower Zn-contaminated region; d.) upper sewage-contaminated zone, below Zn contamination; e.) lower sewage-contaminated zone.

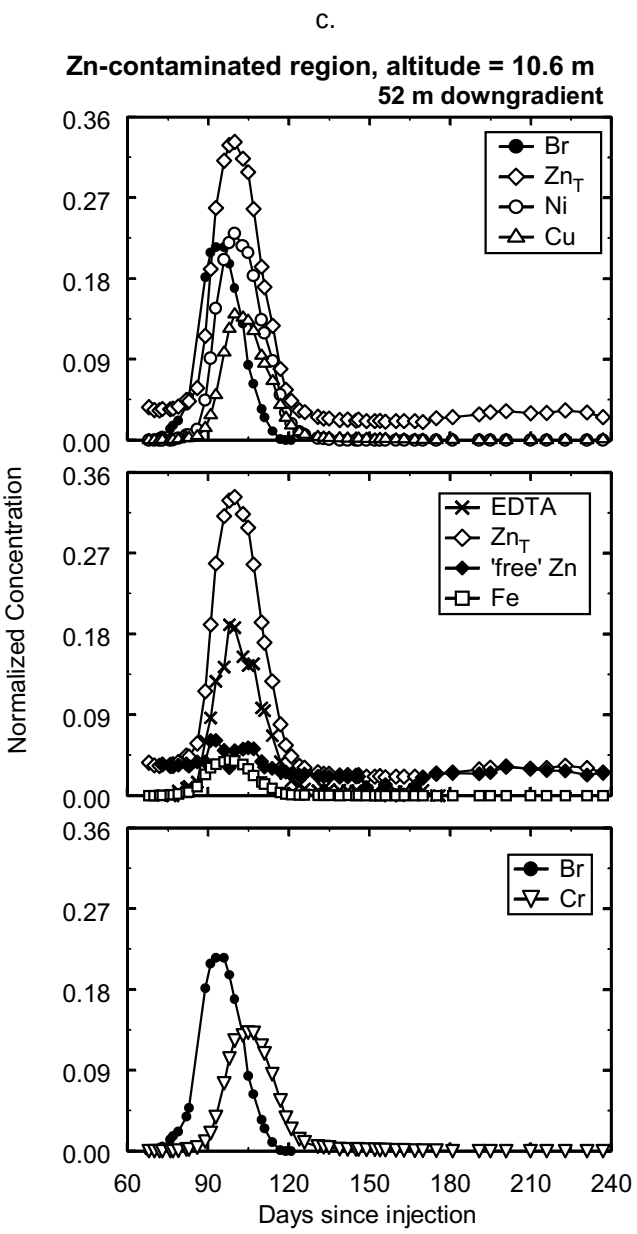

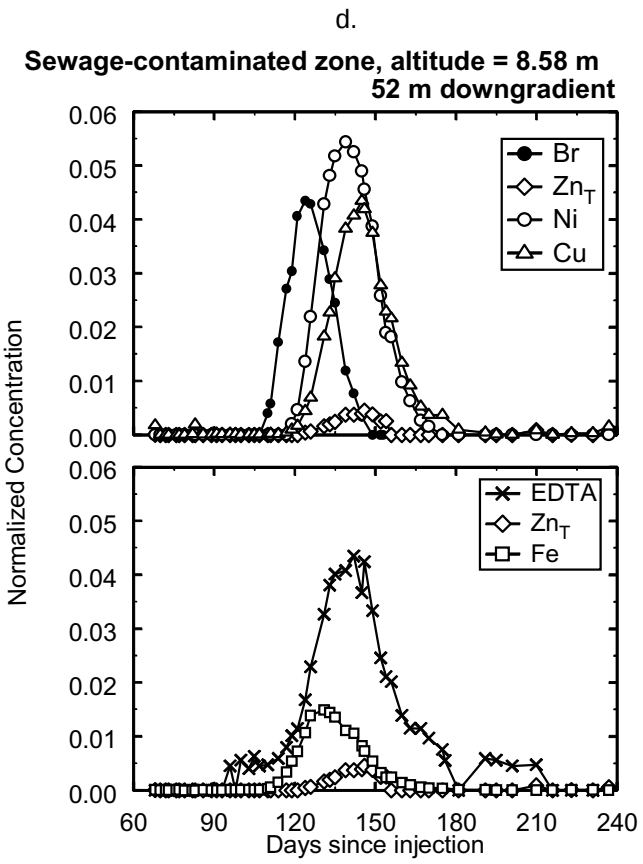

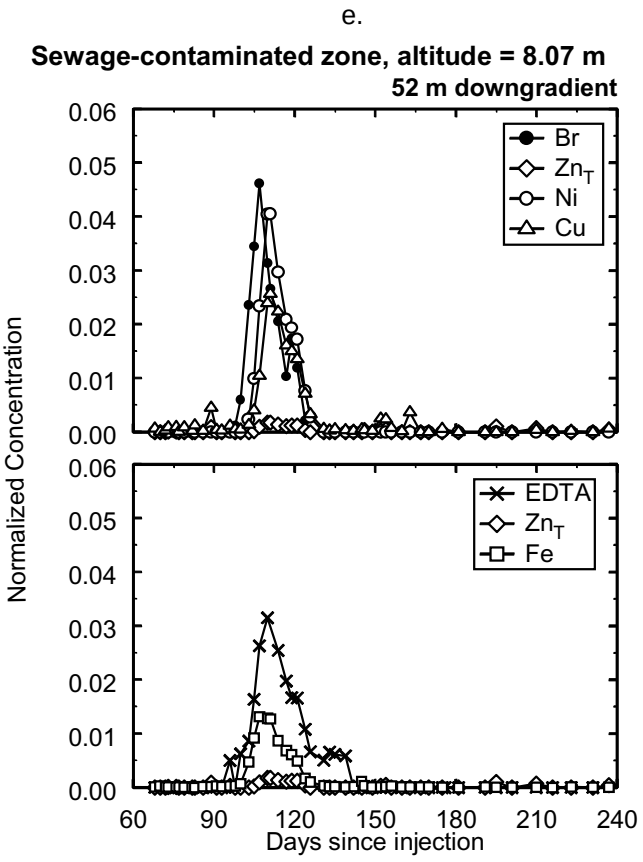

Figure 10. continued.

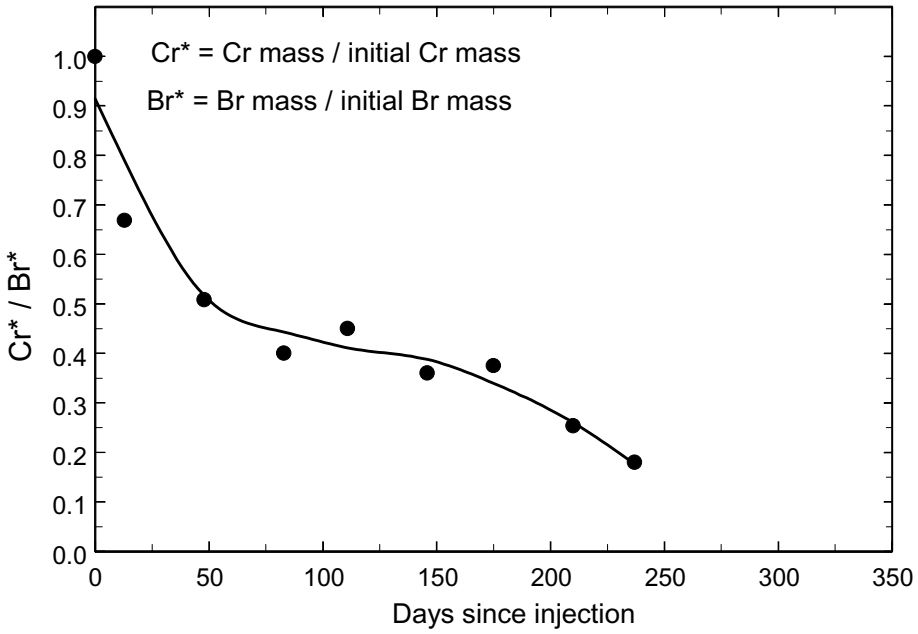

Figure 11. Results of the spatial moments analysis showing the normalized mass of Cr (relative to the injected Cr mass and the normalized Br mass) as a function of time after the injection. The curve shown is a spline fitted to the data points.

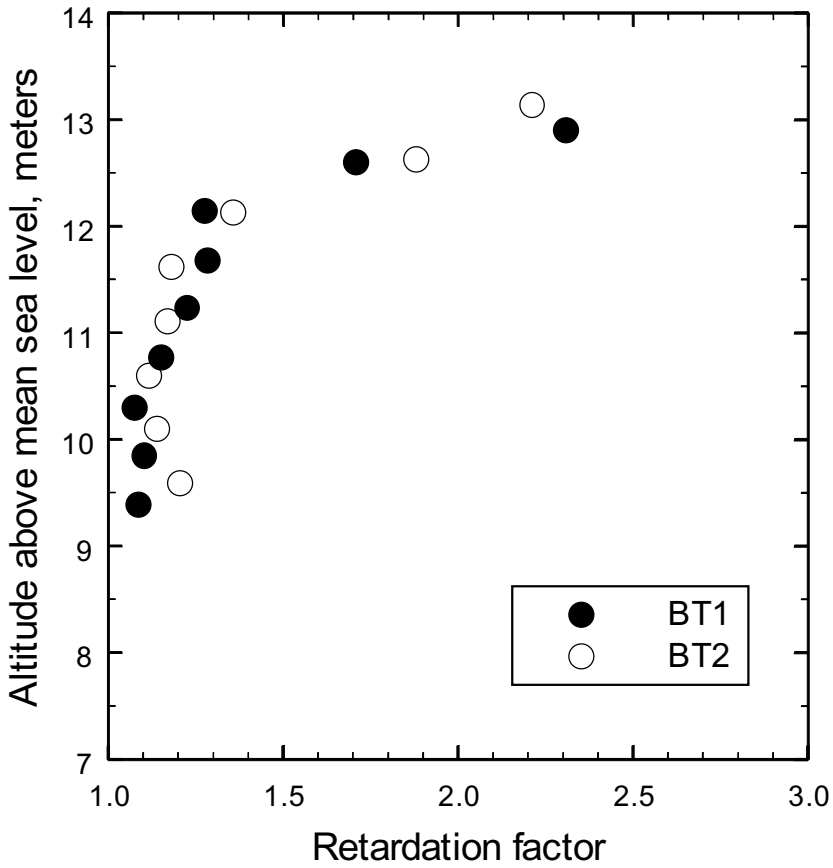

Figure 12. Retardation factors for Cr calculated from the breakthrough-curve data, plotted as a function of the altitude of the sampling port.

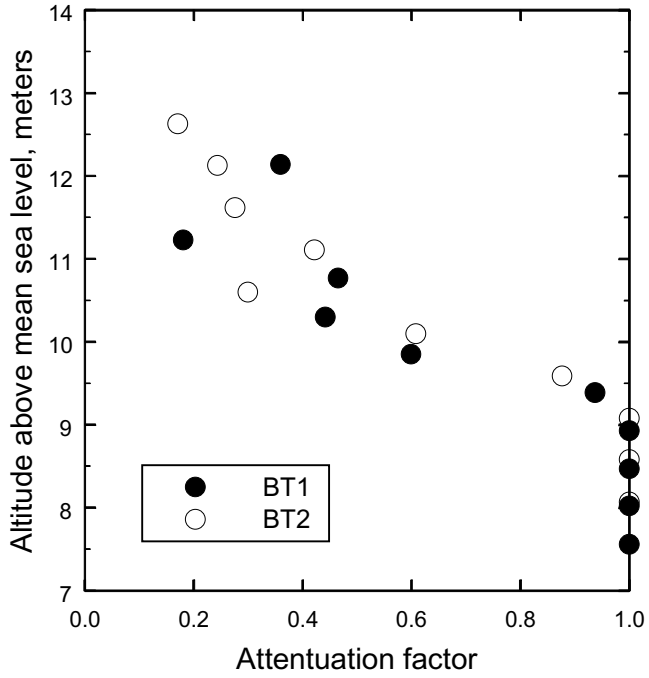

Figure 13. Attenuation factors for Cr calculated from the breakthrough-curve data, plotted as a function of the altitude of the sampling port.

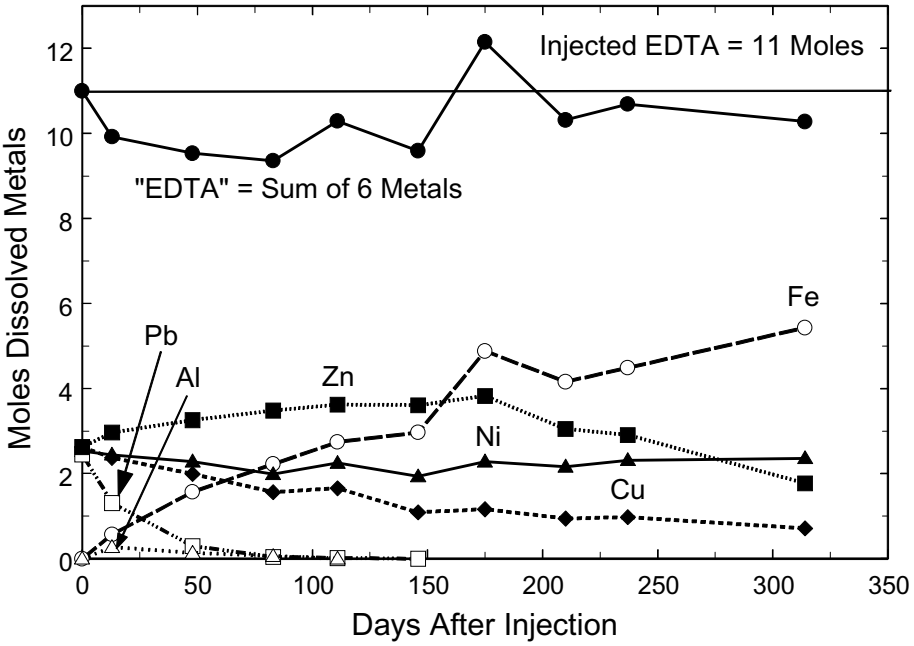

Figure 14. Results of the spatial moments analysis showing the moles of Ni, Pb, Cu, Zn, Fe, and Al in the tracer cloud as a function of time after the injection. The estimated moles of dissolved EDTA in the tracer cloud are shown from the sum of the moles of the six metals at each synoptic sampling.

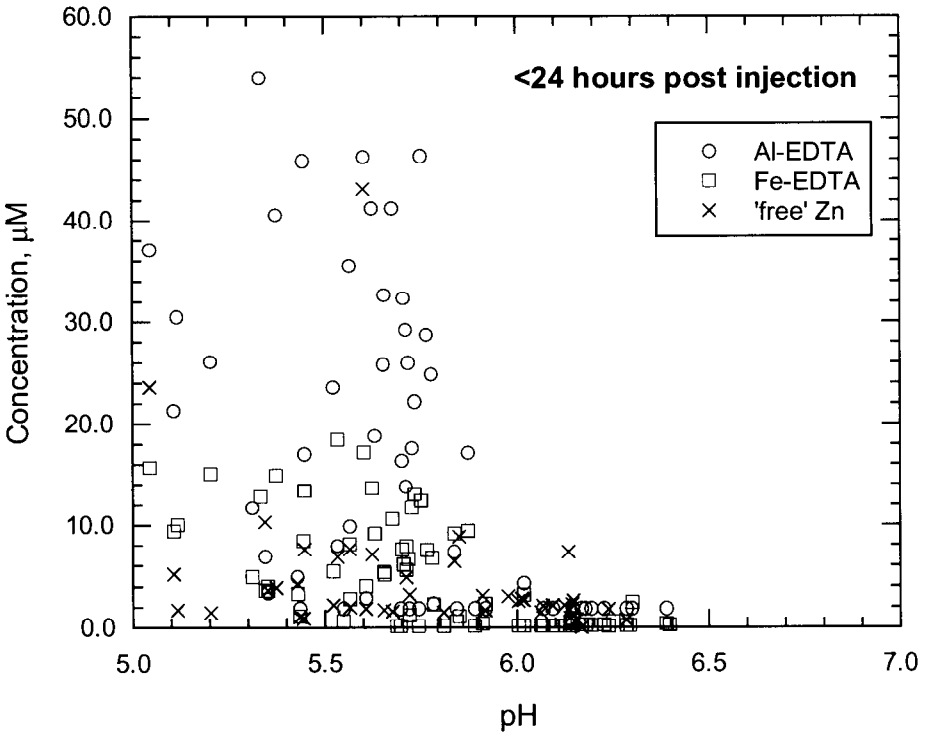

Figure 15. Concentrations of dissolved Al- and Fe-EDTA complexes and uncomplexed (free) Zn as a function of the pH of groundwater samples collected 24 hours after the injection was completed.

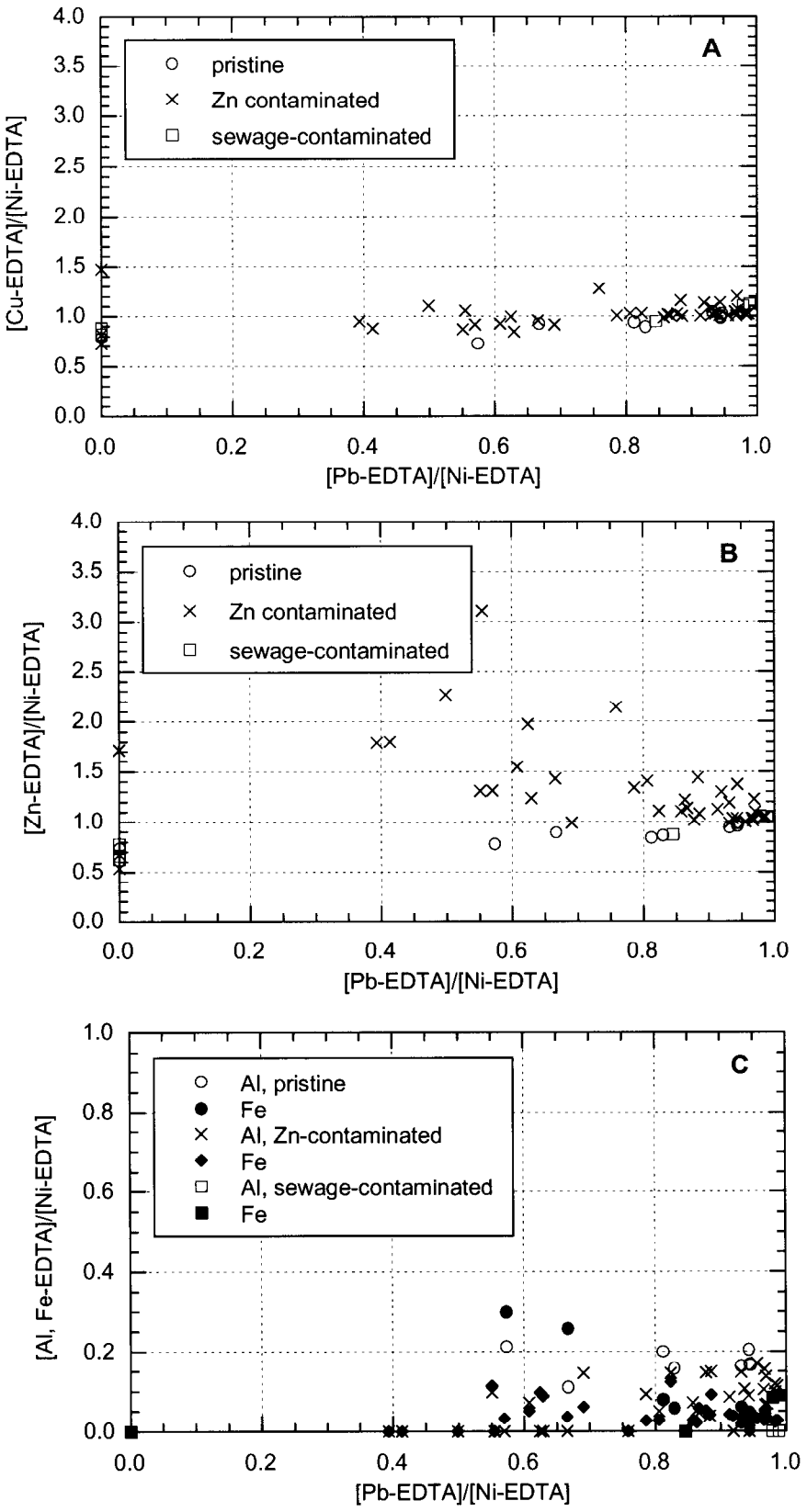

Figure 16. Change in metal-EDTA complexes relative to the amount of Pb-EDTA present for days 1 through 7 after injection. All data is normalized to the amount of Ni-EDTA in the sample. Data is grouped by aquifer zone. (A) Cu-EDTA, (B) Zn-EDTA, and (C) Al- or Fe-EDTA (note scale change).

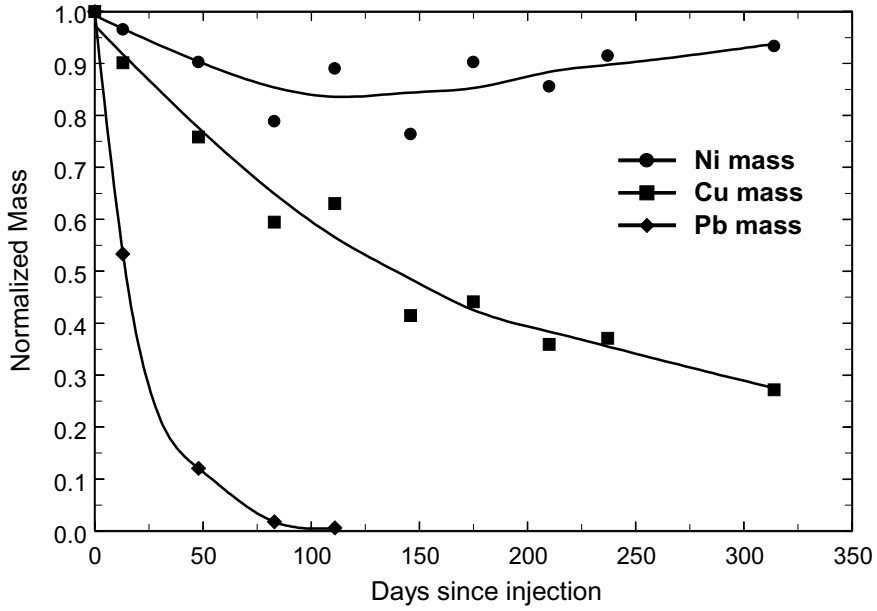

Figure 17. Results of the spatial moments analysis showing the normalized masses of Ni, Cu and Pb (relative to their injected masses) as a function of time after the injection. The curves shown are splines fitted to the data points.

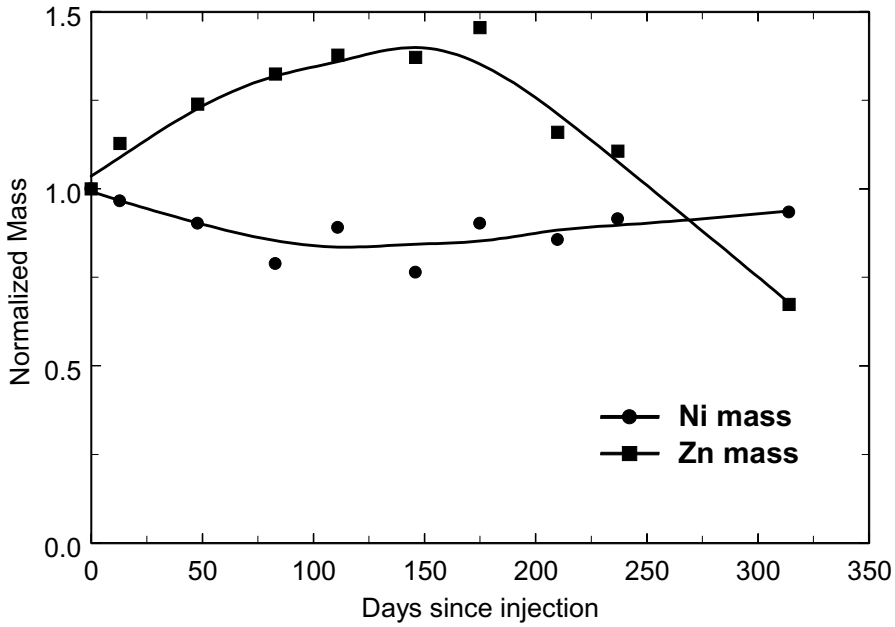

Figure 18. Results of the spatial moments analysis showing the normalized masses of Ni and Zn (relative to their injected masses) as a function of time after the injection. The curves shown are splines fitted to the data points.

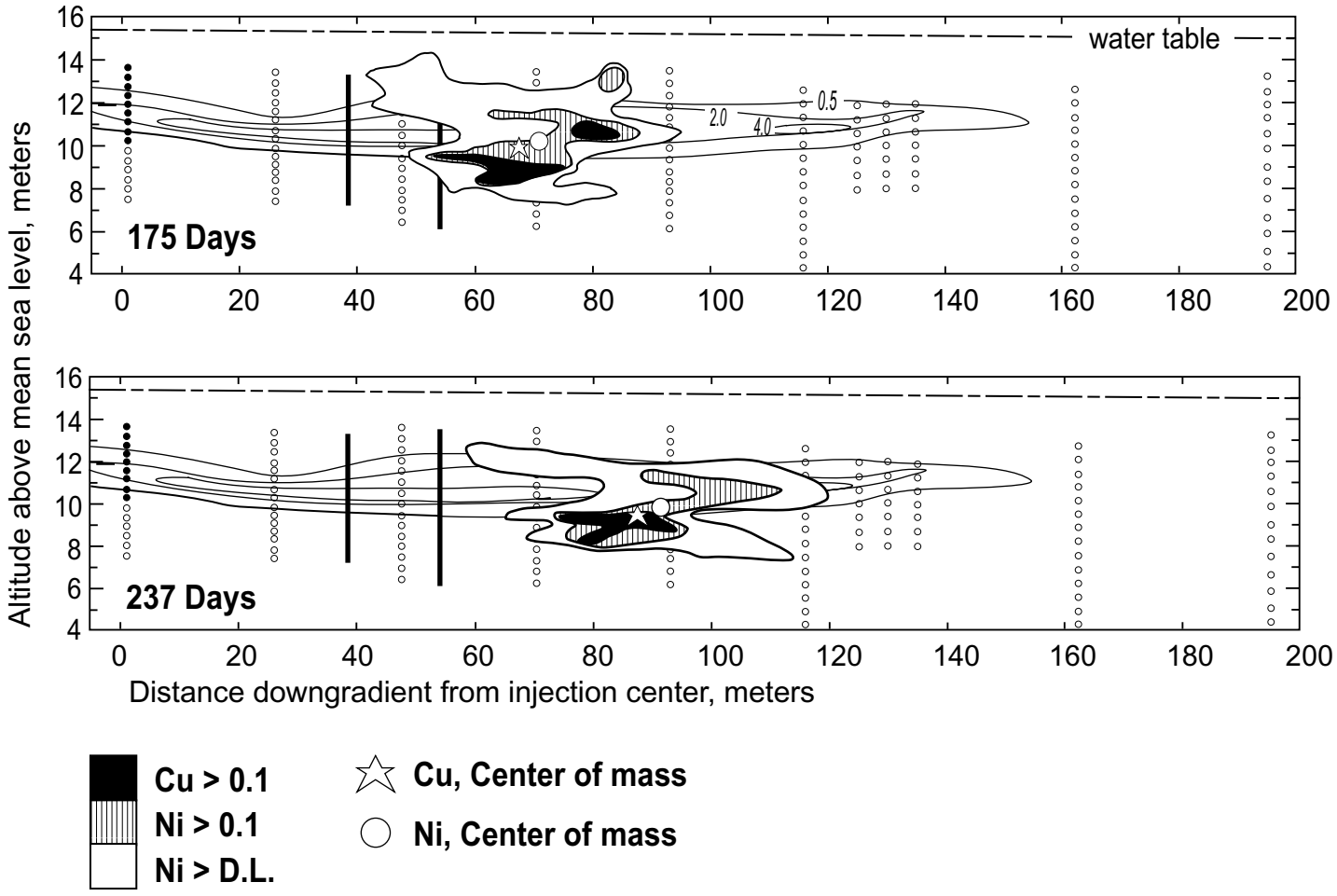

Figure 19. Longitudinal cross section through the portion of the tracer cloud containing metal-EDTA complexes at 175 (upper panel) and 237 days (lower panel) after injection; numbered contours show background Zn concentrations (µM, before injection) as was shown in Figure 4. White area shows the portion of the tracer cloud with Ni concentrations above the detection limit. Regions with vertical lines show where normalized Ni concentrations exceeded 0.1. Black regions show where normalized Cu concentrations exceeded 0.1. Note that in both panels, regions with Ni C/C_0 values > 0.1 enclose regions with Cu C/C_0 values > 0.1. The circle and star show the locations of the centers of mass of Ni and Cu, respectively, from the spatial moments analysis.

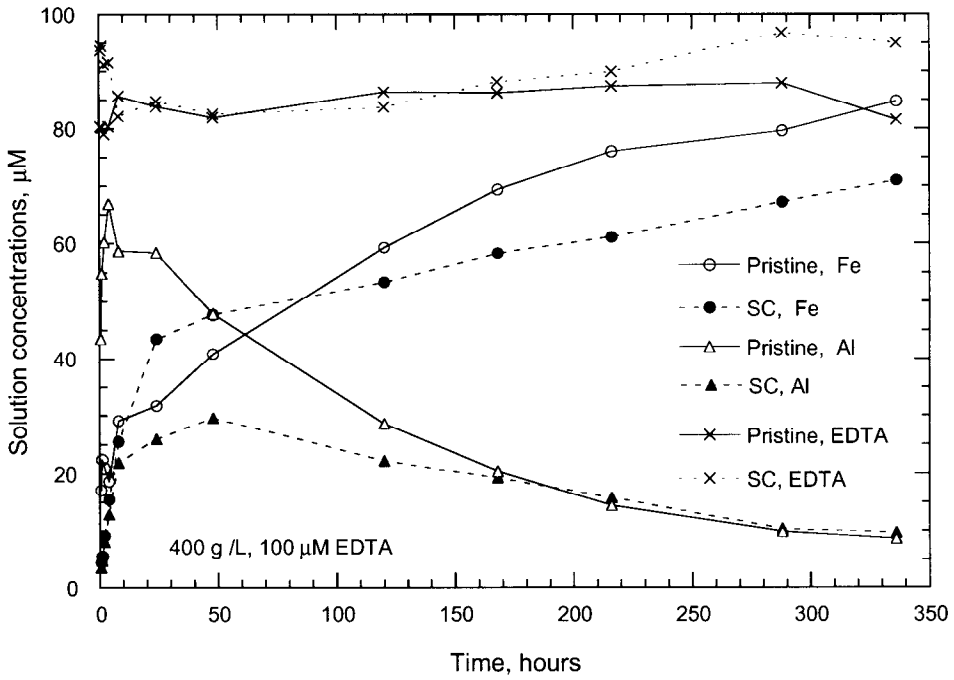

Figure 20. Concentrations of dissolved Fe, Al, and EDTA as a function of time in batch experiments with two samples of composite aquifer sediments mixed with artificial groundwater solutions containing 100 µM EDTA. pH in pristine experiments was 5.4; pH in sewage-contaminated (abbreviated as SC in legend) experiments was 6.5. The concentration of dissolved Al peaks at 4 hours under pristine zone conditions and at 48 hours under sewage-contaminated zone conditions. Dissolution of Fe was still continuing after 336 hours (14 days).

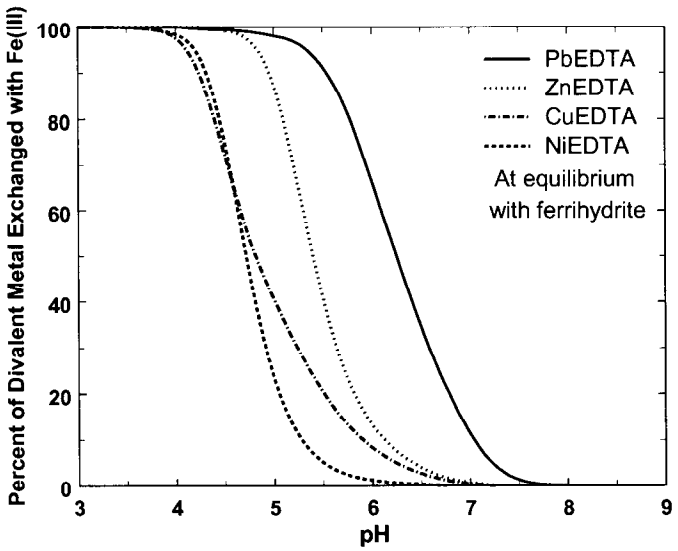

Figure 21. Calculated extents of metal exchange between metal-EDTA complexes and Fe(III) dissolved from ferrihydrite as a function of pH. The calculations assume chemical equilibrium and consider the adsorption of free metal ions (using the constants of Dzombak and Morel, 1990) and the adsorption of metal-EDTA complexes (from fitting the retardation of these complexes in the pristine zone). Calculations are shown for a suspension of ferrihydrite (with equal surface area per liter of water to that of Cape Cod sediments in the aquifer) mixed with sewage-contaminated groundwater containing 250 µM of each metal-EDTA complex, which is close to the conditions just after injection.

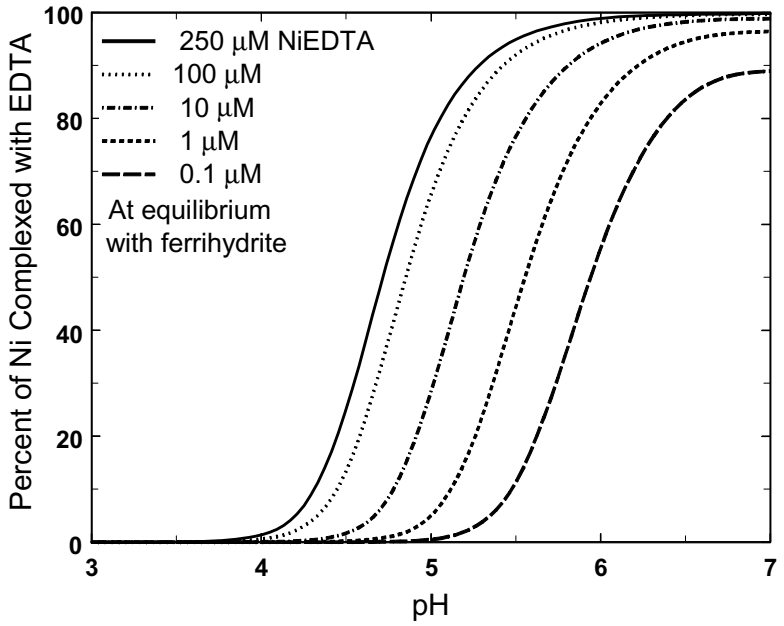

Figure 22. Calculated extents of Ni exchange between Ni-EDTA complexes and Fe(III) dissolved from ferrihydrite as a function of pH and the initial Ni-EDTA concentration. Other conditions in the calculations are the same as those in Figure 21.

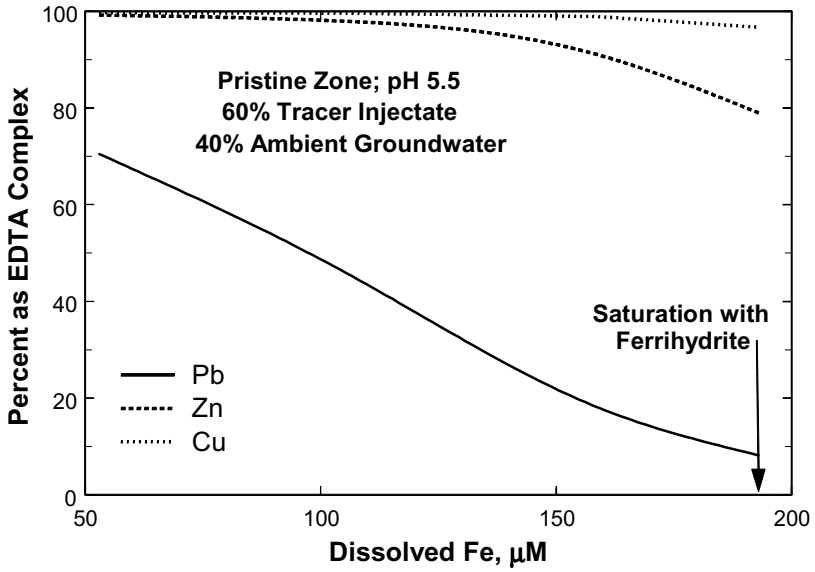

Figure 23. Calculated extents of metal exchange between metal-EDTA complexes and Fe(III) as a function of pH and dissolved Fe(III) concentration. The calculations assume chemical equilibrium (except for ferrihydrite dissolution) and consider the adsorption of free metal ions and metal-EDTA complexes as in Figure 21. Calculations are shown for a solution containing the injectate solution diluted 3:2 with pristine groundwater. Saturation of the solution with respect to ferrihydrite dissolution is achieved at a dissolved Fe concentration near 200 μM.

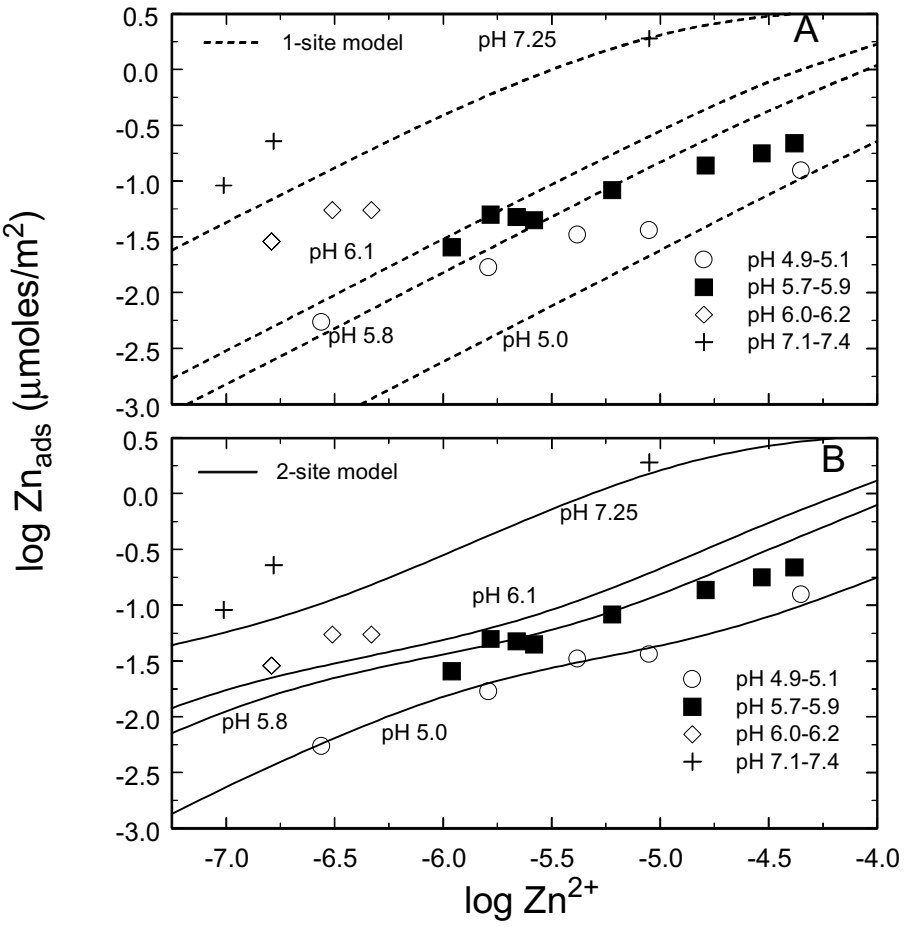

Figure 24. Laboratory batch experimental data for Zn adsorption onto a composite sample of aquifer sediments collected from the site and surface complexation model fits. a) 1-site surface complexation model. b) 2-site surface complexation model. (From Davis et al., 1998.)

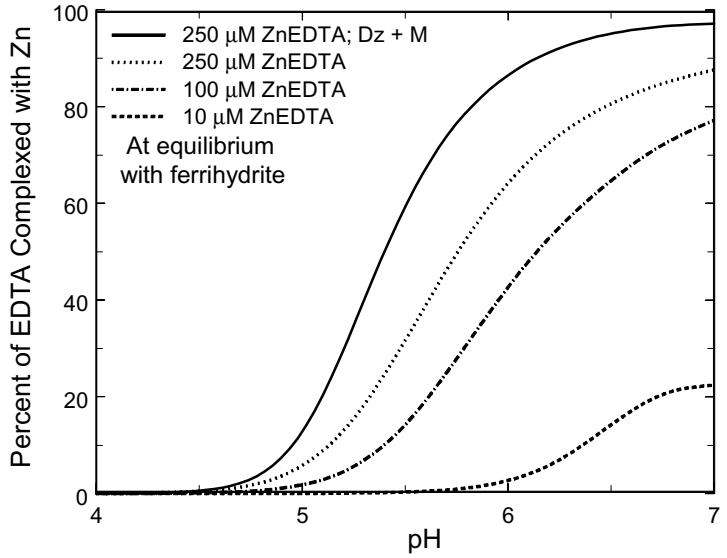

Figure 25. Calculated extents of metal exchange between Zn-EDTA complexes and Fe(III) dissolved from ferrihydrite as a function of pH and Zn-EDTA concentration. The calculations assume chemical equilibrium and consider the adsorption of free Zn ions using the constants derived from batch adsorption data with Cape Cod sediments. Adsorption of Zn-EDTA complexes was considered in the same manner as in Figure 21. For comparison, the curve marked Dz + M shows the calculated extent of exchange at 250 µM Zn-EDTA as shown previously in Figure 21.

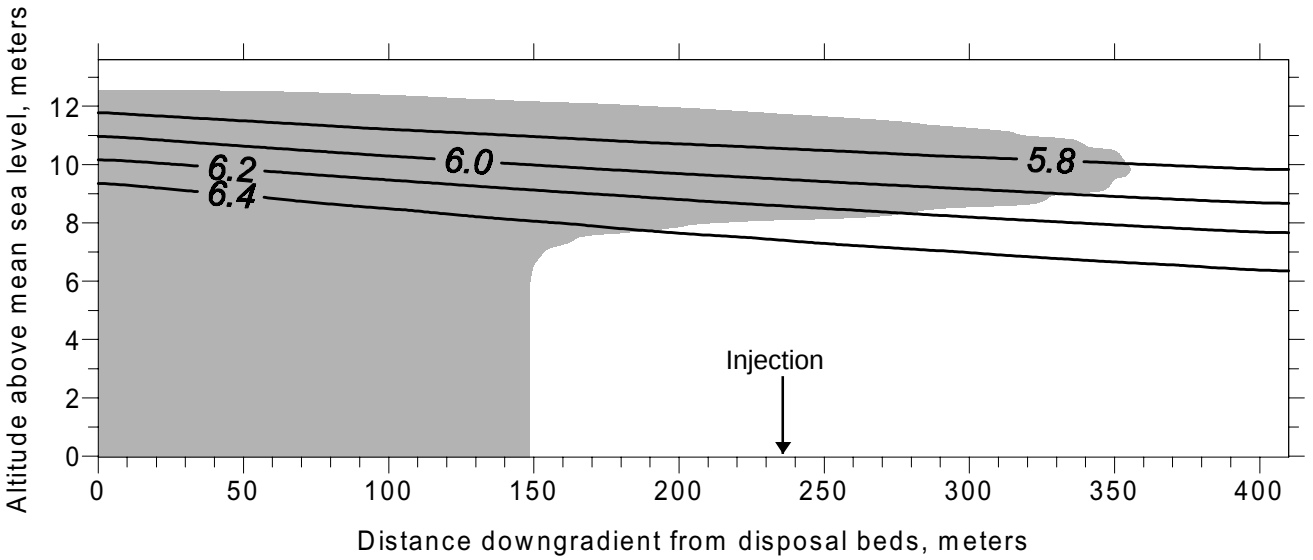

Figure 26. Simulated distribution of dissolved Zn after 60 years. Numbered contour lines show the pH gradient used in the simulation. Shading shows the region where the Zn concentrations were greater than 1 μM. The 0.2 μM contour (analytical detection limit) was within a few meters of that shown, however it was much more strongly affected by numerical oscillations, which are evident in the 1 μM contour near the leading edge. The abscissa shows the distance downgradient from the sewage effluent disposal beds. The injection was located approximately 238 m downgradient from the disposal beds.

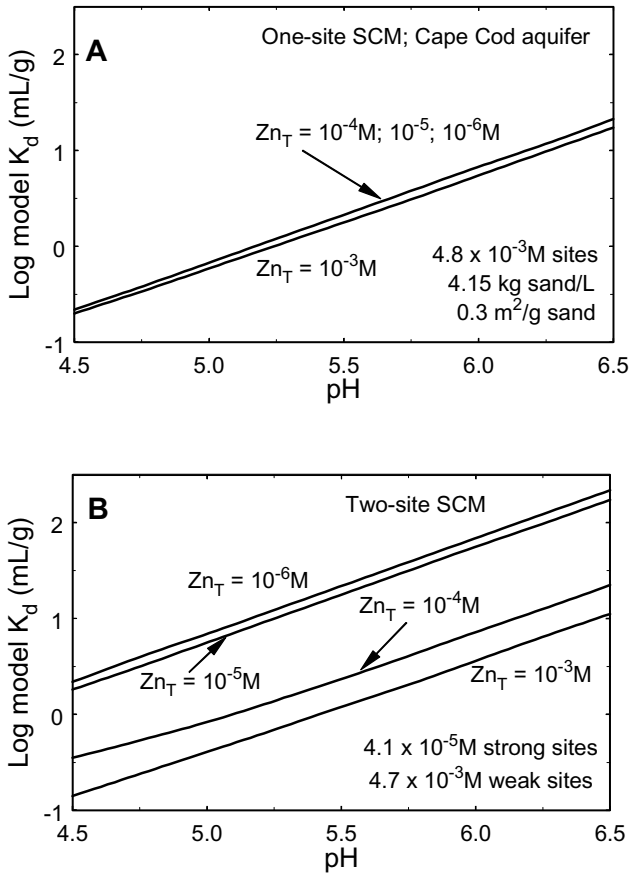

Figure 27. Calculated values of the distribution coefficient, K_d, for adsorption of Zn as a function of pH and total Zn concentration per liter of water in the aquifer using (A) the one-site model for Zn adsorption, and (B) the two-site model (Davis et al., 1998). Solid matrix Zn that is not available for desorption reactions is not included in the definition of total Zn for these calculations.